Gene structure-based homology search identifies highly divergent putative effector gene family

David L. Stern* & Clair Han

Affiliation:

Janelia Research Campus of the Howard Hughes Medical Institute, 19700 Helix Drive, Ashburn, VA 20147, USA

* Corresponding author

Abstract

Homology of highly divergent genes often cannot be determined from sequence similarity alone. For example, we recently identified in *Hormaphis cornu* a family of rapidly evolving *bicycle* genes, which encode novel proteins implicated as plant gall effectors. Sequence similarity search methods yielded few putative *bicycle* homologs in other species. Coding sequence-independent features of genes, such as intron-exon boundaries, often evolve more slowly than coding sequences, however, and can provide complementary evidence for homology. We found that a linear logistic regression classifier using only structural features of *bicycle* genes identified many putative *bicycle* homologs in other species. Independent evidence from sequence features and intron locations supported homology assignments. To test the potential roles of *bicycle* genes in other aphids, we sequenced the genome of a second gall-forming aphid, *Tetraneura ulmi*, and found that many *bicycle* genes are strongly expressed in the salivary glands of the gall forming foundress. In addition, *bicycle* genes are strongly overexpressed in the salivary glands of a non-gall forming aphid, *Acyrthosiphon pisum*, and in the non-gall forming generations of *Hormaphis cornu*. These observations suggest that Bicycle proteins may be used by multiple aphid species to manipulate plants in diverse ways. Incorporation of gene structural features into sequence search algorithms may aid identification of deeply divergent homologs, especially of rapidly evolving genes involved in host-parasite interactions.

Introduction

One challenge that is faced by evolutionary and functional genetic studies is that many genes have been identified as “orphan” or lineage-specific genes because homologous sequences cannot be identified outside of a limited taxonomic range. Many lineage-specific genes may not be truly novel, however, since sequence divergence can cause homologs to become undetectable by sequence-search methods (Vakirlis et al., 2020; Weisman et al., 2020). Identifying such extremely divergent homologs remains a significant bioinformatic challenge and limits functional inferences derived from homology (Loewenstein et al., 2009).

Genes involved in host-parasite systems often evolve extremely divergent sequences as a result of genetic conflict (Eizaguirre et al., 2012; Paterson et al., 2010). Aphids and their host plants represent one such antagonistic pair. Aphids are small insects that feed by inserting their thin mouthparts (stylets) into the phloem vessels of plants to extract nutrients (Dixon, 1978). Like many herbivorous insects, aphids introduce effector molecules into plant tissues to manipulate the physiology and development of plants to the insects’ advantage (Elzinga and Jander, 2013; Hogenhout and Bos, 2011; Mutti et al., 2008; Rodriguez et al., 2017). For example, aphids introduce calcium binding proteins that prevent the plant’s ability to block phloem cell transport in response to phloem vessel damage (Will et al., 2007). It is believed that aphids introduce a wide range of effector proteins and that these molecules contribute to the debilitating effects of multiple aphid species on plants, which imposes significant financial damage on most major agricultural crops (Schaible et al., 2008).

In an extreme form of aphid manipulation of plant physiology and development, some aphid species induce novel plant organs, called galls, which provide the aphids with a ready food source and with protection from the elements and from natural enemies (Giron et al., 2016; Mani, 1964; Shorthouse et al., 2005). Galls can be significant nutrient sinks (Burstein et al., 1994), demonstrating that galling aphids induce both local and long-range changes to plant physiology.

We reported recently that the genome of one species of galling aphid encodes 476 related genes encoding diverse, novel, presumptive effector proteins and many of these proteins contain two cysteine-tyrosine-cysteine motifs (CYC) (Korgaonkar et al., 2021). These genes were therefore named *bicycle* (bi-CYC-like) genes. A genome-wide association study revealed that variation in one *bicycle* gene, called *determinant of gall color* (*dgc*), was strongly associated with a red versus green gall color polymorphism and this genetic polymorphism was associated with strong downregulation of *dgc* in aphids and strong upregulation of a small number of genes involved in anthocyanin production in plant galls. In addition, the majority of *bicycle* genes are strongly upregulated in the salivary glands specifically of the aphid generation that induces galls (the fundatrix). Together with genetic evidence that *dgc* regulates the gall phenotype, the enrichment of *bicycle* genes expressed in fundatrix salivary glands suggests that many *bicycle* genes contribute to gall development or physiology.

The primary amino-acid sequences of Bicycle proteins have evolved rapidly, apparently in response to extremely strong positive selection (Korgaonkar et al., 2021). In preliminary studies, we attempted to identify *bicycle* homologs in other insect species using sequence similarity algorithms such as *BLAST* (Altschul et al., 1990) and

hmmer (Eddy, 2011; Johnson et al., 2010), but identified few putative homologs. It was therefore unclear if *bicycle* genes are a recently evolved family of genes or an ancient family that has evolved highly divergent coding sequences.

Extremely divergent homologs have been identified previously using features of gene structures that evolve more slowly than the coding sequence, such as exon sizes and intron positions (Bazan, 1991; Betts, 2001; Brown et al., 1995), and these characteristics of genes have also proven to be valuable for phylogeny reconstruction (Rokas et al., 1999; Rokas and Holland, 2000; Telford and Copley, 2011; Venkatesh et al., 1999). We noted previously that *bicycle* genes have unusual gene structures containing many micro-exons (Korgaonkar et al., 2021) and we considered the possibility that *bicycle* gene structure may be more conserved than *bicycle* gene sequences. To explore the evolutionary history of *bicycle* genes, we therefore sought a method that would allow identification of highly divergent *bicycle* gene homologs that did not rely on sequence similarity. To accomplish this, we built a logistic regression classifier based only on structural features of *bicycle* genes. We found that this classifier was very accurate, despite the fact that it does not include any sequence information. This classifier identified many highly-divergent *bicycle* homologs in *H. cornu* that could not be identified by sequence similarity search methods, including genes that encode proteins that do not include the previously canonical CYC motif. In addition, the classifier identified many highly divergent candidate *bicycle* homologs in all aphids, phylloxerans, and scale insects we studied. We did not detect any putative homologs in three progressively basal outgroups. Multiple sequence alignment of these putative homologs revealed that many contain N-terminal signal sequences and

CYC motifs, consistent with their assignment as *bicycle* homologs. In addition, gene-structure aware sequence alignment revealed multiple apparently shared intron boundaries between putative homologs that share little obvious sequence similarity. In addition, putative *bicycle* homologs are highly enriched in the salivary gland mRNA of two gall forming and one non-gall forming aphid. All of this evidence supports the hypothesis that *bicycle* gene homologs encode effector proteins in gall-forming and non-gall-forming aphids and also in phylloxerans and scale insects.

Results

***Sequence-based homology searches find few* bicycle *genes outside of* H. cornu**

Bicycle genes in *H. cornu* were identified originally as a subset of previously unannotated genes that were enriched in the salivary gland mRNA of the gall-inducing foundress (Korgaonkar et al., 2021). *Bicycle* genes were found to be the single largest group of such genes that shared sequence similarity. These 476 genes are extremely divergent from one another at the amino-acid sequence level and appear to have evolved rapidly due to positive natural selection. Using sequence-based homology search methods *BLAST* and *hmmer*, we identified a few additional candidate *bicycle* paralogs in *H. cornu* (using *BLAST*) and putative homologs in other aphid species (mainly using *hmmer*). We did not detect any candidate *bicycle* orthologs in genomes from insects of the families Phylloxeridae, Coccoidea, Psylloidea, Aleyrodoidea, and Fulgoroidea (Figure 1).

126

127 ***A classifier based on only gene structural features can identify* bicycle *genes with***
128 ***high probability***

129

130 Sequence-based search methods suggested that *bicycle* genes may be found
131 in other species, but the low number of genes identified, and the incongruence
132 between results from *BLAST* and *hmmer* suggested that sequence-based search may
133 provide low sensitivity to detect *bicycle* homologs (Vakirlis et al., 2020; Weisman et
134 al., 2020). We noticed, however, that while sequence divergence was high at the
135 amino-acid level among *H. cornu bicycle* genes, non-sequence specific features of
136 *bicycle* genes appeared to be relatively well conserved. For example, *bicycle* genes
137 contain a large number of unusually small internal exons (Korgaonkar et al., 2021),
138 making them clear outliers to most genes in the *H. cornu* genome. We also observed
139 that almost all internal exons of *bicycle* genes start with codon position 2, that is, they
140 exhibit exon phase 2 (Figure S1A), which is an extremely different distribution of exon
141 phases compared with other genes in the genome (Figure S1B). Genes containing
142 many exons of similar size all with the same phase are rare in most genomes
143 (Ruvinsky and Watson, 2007).

144 We hypothesized that some aspects of *bicycle* gene structure may evolve
145 more slowly than the primary protein sequences and thus provide an evolutionary
146 signal to detect distantly related *bicycle* homologs (Aguiar et al., 2015). For example,
147 the pattern of exon phases can allow identification of highly-divergent homologous
148 genes (Roy and Gilbert, 2005; Ruvinsky and Watson, 2007). Development of a full

model to characterize gene structure evolution is beyond the scope of this paper, but we explored whether a linear logistic regression classifier could identify *bicycle* homologs based on the following structural features of each gene: length of gene in genome, from start to stop codons; first and last exon length; internal exon mean length; length of the sum of codons; and number of internal exons that start in phase 0, 1, or 2. Since almost all internal *bicycle* exons are of phase 2, there is no additional information from the order of exon phases in *bicycle* genes, and we therefore simply counted the number of exons of each phase.

Characterized *bicycle* genes have an average of approximately 17 and a minimum of 5 exons (Figure S1C), which is strongly different from the genome-wide background (Figure S1D), and Bicycle protein lengths are well explained by total exon number (c.f. Figures S1E and S1F). We excluded all genes with zero or one internal exon to accurately summarize internal exon mean lengths and number of internal exons that start in each of the three phases. Thus, if any *bicycle* genes have evolved to have three or fewer exons, then they could not be detected with this classifier.

The classifier exhibited extremely good performance with all data partitions (Figure S2A) and, therefore, a full model was constructed using all *bicycle* and annotated genes. (Non-annotated genes were excluded from model training and validation because we hypothesized that this set may include additional *bicycle* homologs.) The classifier categorized the vast majority of genes as either non-*bicycle* or *bicycle* genes with high probability (Figure S2B). To decide on a probability cutoff to identify putative *bicycle* homologs, we considered the trade-off between precision (the proportion of true positives among both true and false positives) and recall (the

proportion of true positives among true positives and false negatives). We chose a model probability cutoff that equalized precision and recall (P/R = 1), which yielded precision and recall values of 0.99 (Figure S2C, D).

To determine whether all gene features were required for accurate classification, we removed one factor at a time, retrained the model, and calculated precision and recall values using the same threshold as the full model. We found that no single factor was critical for model performance (Figure S2E), although removal of the number of mode 2 exons resulted in the strongest decrement in model performance, resulting in precision and recall values of 0.98 and 0.96, respectively.

To determine whether any single predictor was sufficient to identify *bicycle* genes with high confidence, we calculated precision and recall values for linear models using one predictor at a time (Figure S2F). Mean internal exon length alone performed best (Figure S2F), consistent with the observation that *bicycle* genes contain an unusually large number of small exons (Figure S3). The number of internal exons in mode 2 also displayed some predictive power on its own (Figure S2F). No other predictors alone had substantial predictive power for discriminating *bicycle* genes from the background (Figure S2F). We observed some level of correlation between predictor variables (Figures S2G-I), but no variables were scalar multiples of each other and we therefore employed the full model using all predictors to search for new *bicycle* genes.

Additional candidate* bicycle *genes can be found in many other species

To search for candidate *bicycle* genes in other species, we applied the classifier to genes from the genomes of twenty-two species spanning the Aphidoidea and species from the five most closely related families, the Phylloxeroidea, Coccoidea, Psylloidea, Aleyrodoidea, and Fulgoroidea (Figure 1). Multiple *bicycle* genes were identified in all Aphidoidea, Phylloxeroidea, and Coccoidea we studied and the *bicycle* genes identified by the classifier encompass 98.2-100% of the *BLAST* identified bicycle genes and 86.8-100% of the *HMMER* identified *bicycle* genes in all species with more than 3 *bicycle* genes. This concordance of methods supports the inference that (1) the classifier has identified *bicycle* homologs and (2) the classifier has higher power than sequence-based approaches to identify *bicycle* genes. As expected from the features of the classifier, the candidate *bicycle* genes in all species exhibited the unusual feature of being encoded by genes containing many micro-exons (Figure S3).

While the classifier exhibits substantial power to detect highly divergent *bicycle* genes across species, the classifier might fail to identify *bicycle* genes with gene structures that are divergent from the *bicycle* genes originally identified in *H. cornu* that were used to train the classifier. In addition, the genomes of many species studied here are highly fragmented, and some true *bicycle* genes may have been annotated with a subset of their exons. We therefore performed profile *hmmer* search within each species starting with the classifier-identified *bicycle* genes in each species (last column in Figure 1). The *hmmer* search identified additional candidate *bicycle* genes in some species, suggesting that the classifier underestimates the number of *bicycle* genes in some species.

218

219 ***Candidate* bicycle *genes in* H. cornu are *highly expressed and share structural***
220 ***homology***

221

222 When we applied the classifier to all genes in the *H. cornu* genome, we identified
223 four false negative and 181 “false positive” genes. Since we chose a probability cutoff
224 that should report an approximately equal number of false negatives and false
225 positives, we hypothesized that the vast majority of “false positives” are newly
226 discovered *bicycle* homologs. We clustered these genes together with the original
227 *bicycle* genes based on sequence similarity (Figure 2A), and found that 528
228 represented a single group of related genes (Cluster 2, Figure 2A) that all share
229 sequence similarity with, and included, the originally defined 476 *bicycle* genes (Figure
230 2C).

231 We also identified a second cluster of 129 genes that encode proteins that do
232 not share strong sequence similarity with the originally defined Bicycle proteins and do
233 not exhibit strong evidence for the CYC motif (Cluster 1, Figure 2A, B). Approximately
234 20 of these genes were strongly enriched in the salivary glands of gall-inducing
235 foundresses, but many of these Cluster 1 genes were strongly enriched in salivary
236 glands of other life stages, especially generations that feed on River Birch (Figure 2D-
237 F). In addition, approximately 20 *bicycle* genes containing the CYC motif (Cluster 2)
238 were weakly expressed in fundatrix salivary gland, but strongly expressed at other life
239 stages (Figure 2E-G).

Like the original 476 *bicycle* genes, the new putative *bicycle* homologs likely experienced increased levels of positive selection. We found that the new putative *bicycle* homologs displayed a similar pattern to the original *bicycle* genes of elevated ratios of non-synonymous (d_N) to synonymous (d_S) substitutions between *H. cornu* and its closely related sister species *H. hamamelidis* compared to the genomic background (Figure S4A-C). In addition, we found that signals of selective sweeps, based on *H. cornu* population site frequencies, are enriched near both the original *bicycle* genes and the newly discovered putative *bicycle* homologs (Figure S4D).

Since some of these new putative *bicycle* homologs shared little apparent sequence similarity with the originally defined *bicycle* genes, we sought additional evidence for homology. We hypothesized that other details of gene structure not employed in the classifier, such as intron positions, might provide additional evidence of shared ancestry. We therefore performed gene-structure-aware multiple sequence alignment of the original *bicycle* genes and the new putative *bicycle* genes identified by the classifier (Gotoh, 2021).

Initial attempts to align all 653 candidate proteins were uninformative and we hypothesized that this was because these proteins display a large range of lengths and exon numbers (Figure S1C). We therefore divided Bicycle proteins of Cluster 2 into four groups based on protein length (blue dotted lines in Figure 3A). Logo plots of these four groups revealed a striking pattern, proteins contain one, two, three, or four CYC motifs (Figure 3B-E), and we therefore call these *unicycle, bicycle, tricycle,* and *tetracycle* genes, respectively. This evolutionary comparison suggests that the CYC motif is a functional unit, which can be multimerized within individual proteins.

We then divided *H. cornu bicycle* homologs into four length categories and performed gene-structure aware protein sequence alignments to search for shared intron position between the originally defined *bicycle* genes and the newly discovered *bicycle* putative homologs of Cluster1. We identified many evolutionarily shared intron positions between the two classes of putative homologs (Figure 5 Supplement 1A-D).

To determine whether more introns are shared between the original *bicycle* genes and newly identified putative *bicycle* genes than expected by chance, for example given an alignment of two groups of unrelated genes, we developed a metric of intron concordance and estimated the null distribution by resampling intron concordance between *bicycle* genes and three unrelated gene families (Figure S6). Intron concordance was measured as the correlation coefficient between the number of introns at each alignment position for one gene family versus the *bicycle* gene family (Figure S6A-D). Unrelated gene families were found to have intron positions distributed approximately randomly relative to *bicycle* genes with mean R close to 0 (Figure S6C, E). In contrast, newly discovered *bicycle* genes, both from *H. cornu* and from other species, displayed positive R much greater than 0 and significantly different from distributions of R values found for pairs of unrelated gene families (Figure S6E). This analysis provides statistically significant support for the conclusion that newly discovered putative *bicycle* genes share introns in the same locations more often than expected by chance between unrelated gene families, and thus, that they are likely *bicycle* gene homologs.

These results provide evidence for several conclusions. First, measures of gene structure alone can reliably identify many, but perhaps not all, divergent *bicycle* genes.

286 Second, some *bicycle* homologs have evolved highly divergent sequences, raising the
287 possibility that highly divergent homologs may be present in other species but are
288 undetectable with sequence-similarity search algorithms. Third, some *bicycle*
289 homologs are highly expressed in salivary glands of non-gall forming life stages,
290 suggesting that some of these proteins may contribute to the effector-protein
291 repertoire outside of the context of gall development. Given these observations, we
292 next tested whether the classifier could identify *bicycle* homologs in a divergent galling
293 aphid species.
294
295 ***Many candidate gall effector genes in* Tetraneura ulmi *are highly divergent***
296 **bicycle *genes***
297
298 There are two major clades of gall forming aphids, the Hormaphididae, to which
299 *H. cornu* belongs, and the Pemphigidae. These two aphid families are thought to have
300 shared a common ancestor that induced galls. Therefore, to determine whether *bicycle*
301 genes were present in the common ancestor of gall forming aphids, we assembled and
302 annotated the genome of *Tetraneura ulmi* (Figure S7A), a gall forming aphid belonging
303 to the Pemphigidae (Álvarez et al., 2013). Details of the genome assembly can be
304 found in Supplementary Methods. We annotated the *T. ulmi* genome using mRNA
305 sequencing reads generated from salivary glands and carcasses of the fundatrix (G1)
306 and G2 generations (Figure S7B).
307 We applied the *H. cornu bicycle* gene classifier to predicted genes of the *T. ulmi*
308 genome and identified 279 candidate *bicycle* homologs (Figure 1). In contrast,

309 sequence-based search using BLAST and *hmmer* identified 1 and 53 candidate
310 homologs at E-value < 0.01, respectively. We clustered the 279 *T. ulmi* genes
311 discovered by the gene-structure based classifier based on their predicted amino acid
312 sequences (Figure 4A) and identified three clusters that included proteins with clear
313 evidence for CYC motifs (Figure 4B-D). One cluster of 94 genes does not exhibit clear
314 CYC motifs (Figure 4E). The extreme sequence divergence of these genes within *T.*
315 *ulmi* is supported by the fact that profile *hmmer* search recovered only 69 of these
316 original 279 genes (Figure 1). To test whether these genes likely shared a common
317 ancestor, we performed gene-structure aware alignments of proteins with and without
318 CYC motifs and identified more shared introns between putative homologs with and
319 without CYC motifs (Figure S7C) than expected by chance (Figure S6E). Thus, the *T.*
320 *ulmi* genome contains apparent *bicycle* genes that have become essentially
321 unrecognizable as *bicycle* homologs at the sequence level.

322 To explore whether the *T. ulmi bicycle* genes, and especially the divergent
323 putative *bicycle* homologs, might act as effector proteins, we dissected salivary glands
324 from fundatrices and compared mRNA expression levels in salivary glands versus
325 carcasses. Almost all of the *bicycle* homologs detected by the classifier are amongst
326 the most strongly over-expressed genes in the fundatrix salivary glands (Figure 4F),
327 suggesting that they may contribute to the effector protein repertoire in *T. ulmi*.

328 The discovery of *bicycle* genes in *T. ulmi* using the gene-structure based
329 classifier provides evidence that the classifier can identify putative *bicycle* homologs
330 even when the genes cannot be identified using sequence-based homology methods
331 and that *bicycle* genes were likely present in the common ancestor of gall-forming

aphids. We therefore next tested whether the classifier can detect putative *bicycle* homologs in an aphid species that does not induce galls.

The pea aphid* (Acyrthosiphon pisum) *genome includes many* bicycle *homologs that are candidate effector proteins

The gene-structure based classifier detected 121 putative *bicycle* homologs in the genome of *Acyrthosiphon pisum*, a species that does not induce galls (Li et al., 2019; Richards et al., 2010). In contrast, sequence-based search using *BLAST* and *hmmer* identified 1 and 3 candidate hits at E-value < 0.01, respectively. Multiple sequence alignment of the 121 *A. pisum* putative *bicycle* homologs revealed that most of these genes encode proteins with N-terminal secretion signal sequences and a single CYC motif (Figure 5A). Gene structure aware alignment identified more shared introns between *H. cornu bicycle* genes and *A. pisum* putative *bicycle* homologs (Figure S8) than expected by chance (Figure S6E), providing independent confirmation that these genes shared a common ancestor.

To explore whether these *A. pisum bicycle* homologs may contribute to the effector gene repertoire of *A. pisum*, we performed RNA-seq of salivary glands and carcasses. We found that 55% of the putative *bicycle* genes are among the most strongly overexpressed genes in salivary glands, along with a similar number of additional unannotated genes with signal peptides (Figure 5B). In addition, 17 proteins encoded by genes with multiple microexons were identified by a previously-published proteomic study of proteins secreted by *A. pisum* into an artificial food medium

(Dommel et al., 2020), and we found that at least 13 of these proteins are *bicycle* homologs (Table S1). In summary, the *A. pisum* genome encodes approximately 121 *bicycle* homologs that may contribute to the *A. pisum* effector protein repertoire.

Bicycle genes are present in genomes of aphids, phylloxerids, and coccids

The presence of *bicycle* homologs in three divergent aphid species, *H. cornu*, *T. ulmi*, and *A. pisum* implies that *bicycle* genes were present in the common ancestor of aphids, which lived approximately 280 MYA. To further explore the origins and evolution of *bicycle* genes, we downloaded genomes and RNA-seq data for nine additional aphid species and ten outgroup species from NCBI. We annotated predicted genes in all genomes using the same bioinformatic pipeline that we have used previously to discover *bicycle* genes in other species, applied the *bicycle* gene classifier to all predicted genes, and manually annotated all putative *bicycle* homologs guided by RNA-seq data. One caveat of this analysis is that many of these genomes are fragmented into many contigs and genes bridging contigs are often misannotated or not annotated, resulting in possible under-counting of *bicycle* homologs. In addition, we detected multiple putative *bicycle* homologs near the ends of contigs, suggesting that parts of single *bicycle* homologs are present on multiple contigs, which would lead to over-counting *bicycle* gene homologs. While these problems with current annotations are expected to increase variance in estimates of *bicycle* homologs, we did not detect a dependence of number of *bicycle* homologs detected on genome assembly quality (Figure S9A). In addition, we employed chromosome-level genome

assemblies for two outgroup species where no predicted *bicycle* genes were found, *P. venusta* (Y. Li et al., 2020) and *T. vaporariorum* (Xie et al., 2020), suggesting that the failure to identify *bicycle* genes in these species did not result from poor genome assemblies.

We estimated the phylogeny for these 22 species using whole-genome proteomic predictions (Emms, 2019), and this phylogeny is in general agreement with earlier studies based on a small number of genes (Johnson et al., 2018; Nováková et al., 2013; von Dohlen and N. A. Moran, 1995) (Figure 1). We detected putative *bicycle* homologs in all aphid species studied here, supporting the inference that *bicycle* genes were present in the common ancestor of aphids (Figure 1). We found extensive variation in the number of *bicycle* genes between species. In all aphid species with a sufficient number of *bicycle* homologs, multiple sequence alignment revealed the presence of CYC domains (Figure S9B-E). In most Aphidini species (e.g. *M. persicae*, *A. pisum*, *P. nigronervosa*), most homologs appear to be *unicycle* genes (Figure S9B-C). In *Cinara cedri*, many homologs appear to be *tetracycles* (Figure S9E).

We found 69 putative *bicycle* homologs in *Daktulosphaira vitifoliae* indicating that *bicycle* genes were present in the common ancestor of the Aphidomorpha (Aphidoidea + Phylloxeridea). We also found 74, 26 and 2 putative *bicycle* homologs in the coccid species *Maconellicoccus hirsutus*, *Phenacoccus solenopsis*, and *Ericerus pela*, respectively. In *M. hirsutus* and *E. pela* profile *hmmer* search with the classifier identified genes identified 17 and 12 additional candidate *bicycle* genes, respectively. The putative *bicycle* homologs from these non-aphid species do not contain obvious CYC motifs (Figure S10A-C). However, gene structure aware alignment with the *H.*

401 *cornu bicycle* genes revealed that the putative homologs from *D. vitifoliae*, *M. hirsutus*,
402 and *P. solenopis* share more introns in the same locations with *H. cornu bicycle* genes
403 (Figure S10D-F) than expected by chance (Figure S6E), supporting the inference that
404 these are *bicycle* homologs.

405 We did not detect *bicycle* homologs in any of the species sampled from the
406 Psylloidea, Aleyrodoidea, or Fulgoroidea. These results indicate that *bicycle* genes
407 were present in the common ancestor of coccids and aphids and may have evolved in
408 the common ancestor of these lineages. However, for at least two reasons we cannot
409 rule out the possibility that *bicycle* genes originated earlier. First, we observed
410 extensive variation in the number of *bicycle* homologs across lineages, so *bicycle*
411 genes may have been lost in the specific outgroup species studied here. Second,
412 ancestral *bicycle* genes may not display the specific gene structure detected by our
413 classifier. Deeper taxonomic sampling and other homology search approaches may
414 reveal an older origin of *bicycle* genes.

415

416 **Aphid genomes contain a conserved *megacycle* gene**

417

418 In many of the aphid genomes we studied, our classifier identified a single
419 extremely large gene containing more than 100 microexons and encoding a protein of
420 approximately 2000 amino acids as a candidate *bicycle* homolog (Figure 6A). Since this
421 gene was so large and most existing aphid genomes are incompletely assembled, we
422 observed that many of these gene models were incomplete. We therefore performed
423 *de novo* transcript assembly for all species studied using TRINITY (Grabherr et al.,

2011) and manually assembled consensus transcripts of these long candidate *bicycle* genes.

Since we had previously found that *bicycle* gene length is correlated with the number of encoded CYC motifs (Figure 3), we explored whether these genes encoded proteins with multiple repeating units. Using Rapid Automatic Detection and Alignment of Repeats (Heger and Holm, 2000) via EMBL-EBI (Madeira et al., 2019), we found that these large proteins contain an N-terminal secretion signal and many repeating motifs and each motif is approximately the size of two CYC motifs. This structure was most obvious for the *Melanaphis sacchari* gene (Figure 6A). Sequence-based alignment of 15 predicted repeats of the *M. sacchari* protein, which did not use information of intron positions, revealed multiple shared intron locations across repeats (Figure 6B). Thus, this protein appears to have evolved through multiple internal tandem duplications. This large protein exhibited little obvious sequence similarity to *bicycle* genes, but gene-structure aware alignment revealed multiple apparently conserved intron positions shared between the internal duplications of the large gene from *M. sacchari* and *H. cornu bicycle* genes (Figure S11A), suggesting that they share a common ancestor.

These large genes appear to be divergent Bicycle proteins that have duplicated the core motif many times. We therefore call these *megacycle* genes. Compared to most *bicycle* genes, *megacycle* orthologs are relatively well conserved across aphids and a phylogenetic tree reconstructed from the inferred Megacycle proteins is similar to the aphid phylogeny estimated from the whole proteome (Figure S11B). Most aphid genomes we examined contain a single copy of this gene; we did not detect this gene

in *Diuraphis noxia*, and we found three paralogs in both *Cinara cedri* and *Tetraneura ulmi*. No *megacycle* orthologs were found in any of the non-aphid species.

For the three species for which we have good salivary gland transcriptomic data, *H. cornu*, *T. ulmi,* and *A. pisum* the *megacycle* genes are strongly expressed in salivary glands (Figure 6C-E). Thus, *megacycle* genes may contribute to the effector protein repertoire in aphids. The relatively conserved lengths and sequences of *megacycle* homologs suggests that they may share a relatively conserved role across aphids.

Discussion

Some gene features, such as the structure of the encoded protein or the intron-exon structure of the gene, can provide evidence for homology that is independent of sequence (Bazan, 1991; Betts, 2001; Brown et al., 1995). This source of information is becoming increasingly available with the recent availability of many well-assembled, annotated genomes. It is possible to conceptualize a model that jointly utilizes both sequence and exon-intron structure in homology search, but we realized that *bicycle* genes are encoded with extremely unusual intron-exon structures and that a model incorporating only general features of exons may allow detection of distant homologs.

We found that a linear classifier using information on gene length, exon sizes, exon numbers, and exon phases provided a highly accurate predictor of *bicycle* homologs that could not be identified using sequence similarity searches. This predictor allowed identification of *bicycle* homologs across aphids and in several

470 outgroup taxa (Figure 1). Homology was supported by *post hoc* observation of CYC
471 motifs and of an excess of shared introns across many homologs. Thus, sequence
472 independent features provide substantial evidence of homology and integration of even
473 a few sequence independent features into existing sequence-based search methods
474 may substantially increase power to detect ancient homology relationships between
475 genes. All gene structure features that we used contributed to classifier performance,
476 but no single feature was critically important for classifier performance. Therefore, in
477 future work it would be ideal to incorporate multiple features of gene structure into
478 homology search models.

479 For several reasons, our classifier may have underestimated the number of
480 *bicycle* homologs in each species. First, this approach is sensitive to the quality of
481 genome annotation, which is itself dependent on genome assembly quality. We found
482 that most automatically annotated gene models of *bicycle* genes required manual re-
483 annotation. Thus, we may have overlooked additional *bicycle* genes in these genomes
484 because of genome fragmentation and inaccurate automated gene annotation.
485 Second, *bicycle* gene annotation in most species is likely hampered by the lack of
486 salivary gland RNA-seq samples. We observed considerable variation in *bicycle* gene
487 expression levels among samples, and deep sequencing of diverse samples is likely
488 required to provide sufficient RNAseq evidence to build accurate *bicycle* gene models.
489 Finally, it is possible that some *bicycle* homologs have evolved both divergent
490 sequences and novel gene structures, preventing identification with any existing
491 method.

492

493 **bicycle *genes are not strictly associated with gall formation***

494

495 *Bicycle* genes were detected originally as putatively secreted proteins strongly
496 expressed in the salivary glands of the gall-forming aphid generation of *H. cornu* and
497 variation in one *bicycle* gene is genetically associated with gall color (Korgaonkar et al.,
498 2021). These observations led to the hypothesis that many *bicycle* genes participate in
499 gall development. Our observations provide a revised assessment of potential Bicycle
500 protein functions.

501 First, we found that many *bicycle* genes are most strongly expressed in salivary
502 glands of generations of *H. cornu* that do not induce galls (Figure 2D-F). Second, two
503 of the aphids studied here, *H. cornu* and *T. ulmi*, induce complex galls and their
504 genomes include many more *bicycle* genes than other species we examined, but the
505 genomes of two other gall-forming species, *E. lanigerum* and *D. vitifoliae* have only 27
506 and 69 *bicycle* genes, respectively. In addition, the genomes of some non-galling
507 aphids have many *bicycle* genes, such as *Myzus persicae* and *A. pisum*, with 117 and
508 121, respectively. Thus, across species there does not appear to be a strong
509 correlation between the number of *bicycle* genes and the gall-forming habit.

510 Given these new observations, we hypothesize that if Bicycle proteins have
511 conserved molecular functions, then they likely have different targets in different plant
512 species. In some cases, the targets may induce patterned cell proliferation, resulting in
513 galls, and in others the targets may alter plant physiology in more cryptic ways to
514 confer benefits on aphids.

None of the three coccid species we studied here induce galls. However, many coccids induce depressions, swellings, or other changes in plant organs (Beardsley and Gonzalez, 1975), including the induction of elaborate galls (Cook and Gullan, 2004). Parr (Parr, 1940) reported a remarkable series of experiments that appear to demonstrate that extracts of salivary glands of a coccid are sufficient to induce pit galls on oak trees. It may be worth exploring the hypothesis that *bicycle* genes contribute to the effector gene repertoire of scale insects and especially of the gall-forming species.

New experimental opportunities provided by the presence of* bicycle *genes in many species

One of the challenges with studying the function of *bicycle* genes is that initially they were thought to be restricted to the non-model gall-forming insect *H. cornu*. *H. cornu* displays a complex life cycle, exhibiting many polyphenic forms and migration between two trees every year (Korgaonkar et al., 2021), and prospects for laboratory rearing and subsequent experimental manipulations of this species were poor.

The discovery of *bicycle* genes in other insects opens up the possibility that the function of *bicycle* genes can be studied in species more amenable to laboratory manipulation. For example, RNAi allows gene knockdown in *M. persicae* (Chen et al., 2020; Coleman et al., 2015; Gao et al., 2021; Mathers et al., 2017; Niu et al., 2019; Pitino et al., 2011) and *A. pisum* (Han et al., 2006; Mutti et al., 2008, 2006; Niu et al., 2019; Shakesby et al., 2009; Vellichirammal et al., 2017; Will and Vilcinskas, 2015) and CRISPR-Cas9 mutagenesis allows gene knockout in *A. pisum* (Le Trionnaire et al.,

538 2019). Thus, the discovery of many bicycle genes in these species presents new
539 experimental opportunities to uncover the organismal and molecular functions of
540 *bicycle* genes.

Methods

Gene structure based bicycle *gene classifier*

The *bicycle* gene classifier was built as a generalized linear model (GLM) with the following predictor variables: total gene length, total length of coding exons, first coding exon length, last coding exon length, mean internal exon length, and number of internal exons in phase 0, 1, and 2. All length measurements are in base pairs. All genes with zero or one internal exon were removed from the training and test datasets because mean internal exon lengths and number of internal exons starting in each of the three phases cannot be accurately estimated, hence our classifier was unable to detect any potential *bicycle* genes with only one to three exons. The dependent variable from the GLM is the predictor of *bicycle* gene classification. The GLM was implemented with the *glm* function as *binomial* with *logit* link, and response variables for the whole-genome gene set were predicted using *predict*, both in the *R* base package *stats* v.3.6.1.

In the training set, the dependent variable of the GLM is whether the transcript was previously classified as a *bicycle* gene (Korgaonkar et al., 2021), where *bicycle* genes were coded as 1 and non-bicycle genes were coded as 0. We used only genes classified as either *bicycle* genes or previously annotated genes in the training set due to the possibility that unannotated genes include additional previously undetected *bicycle* genes. Previous annotation was defined as having at least one significant match at $E < 0.01$ after Bonferroni correction for multiple searches with *blastp* (*blast* v.2.9.0), *blastx* (*blast* v.2.9.0), or *hmmscan* (*HMMER* v3.2.1) against the Pfam database.

We evaluated the performance of the classifier using a precision-recall curve where $precision = \frac{TP}{TP+FP}$ and $recall = \frac{TP}{TP+FN}$, where TP, FP, and FN are the number of true positives, false positives, and false negatives, respectively. To determine a cutoff value on the dependent variable of the GLM for *bicycle* gene classification, we tested all possible cutoffs from 0 to 0.98 in increments of 0.02 to find the cutoff resulting in a precision to recall ratio closest to 1. We first validated our model by repeatedly sampling and training on 70% of the data and testing on the remaining 30% of the data for 100 replicates and found no substantial change to the trained classifier or the resulting cutoff value (mean 0.7338, s.d. 0.1578) amongst replicates. We therefore trained the final classifier on all *H. cornu bicycle* genes and annotated non-*bicycle* genes without subsampling and determined a cutoff value of 0.72 (precision = 0.9925, recall = 0.9925). The coefficients to the independent variables in the GLM are as follows: intercept = 6.26, total exon length = -0.0206, total gene length = -0.0000642, first exon length = -0.00632, last exon length = 0.0103, mean exon length = -0.0655, number of exons in phase 0 = -3.32, phase 1 = -1.12, and phase 2 = 1.21. We evaluated the contribution of each independent variable by training the *H. cornu* dataset using GLMs with each term removed one at a time. We applied the GLM trained by the *H. cornu* dataset to twenty-one other species belonging to the families of Aphidoidae, Phylloxeroidae, Coccoidea, Psylloidea, Aleyrodoidea, and Fulgoroidea.

Aphid collections and dissections

Aphids of *Tetraneura ulmi* were collected from galls collected on *Ulmus americana* on the grounds of Janelia Research Campus (Table S2-3). Aphids of *A. pisum* LSR1 were kindly provided by Greg Davis and grown on broad bean plants in the laboratory. Salivary glands

were dissected out of multiple instars of fundatrices and their offspring for *T. ulmi* and of virginoparae for *A. pisum* and stored in 3 uL of Smart-seq2 lysis buffer (0.2% Triton X-100, 0.1 U/mL RNasin Ribonuclease Inhibitor) at -80°C for later mRNA isolation. Carcasses of both species were ground in PicoPure extraction buffer and mRNA was prepared using the PicoPure mRNA extraction kit. RNAseq libraries were prepared as described previously (Korgaonkar et al., 2021).

Genome sequencing, assembly, and annotation of Tetraneura ulmi

HMW gDNA was prepared from *T. ulmi* aphids isolated from a single gall following the Salting Out Method provided by 10X Genomics (https://support.10xgenomics.com/genome-exome/sample-prep/doc/demonstrated-protocol-salting-out-method-for-dna-extraction-from-cells). 10X linked-read libraries were prepared and Chromium sequencing was performed by HudsonAlpha Institute for Biotechnology. Genomes were assembled with *Supernova* v.2.1.0 commands *run* and *mkoutput* (Weisenfeld et al., 2017).

We used 133,280,000 reads for an estimated raw genome coverage of 56.18X. The genome size of the assembled scaffolds was 344.312 Mb and the scaffold N50 was 10 Mb. Using BUSCO completeness analysis with *gVolante* version 1.2.0 and BUSCO_v2/v3 (Nishimura et al., 2017), we found that the genome contains 1035 of 1066 (97.1%) completely detected core arthropod genes and 1043 of 1066 (97.8%) partially detected core genes. The genome was annotated for protein-coding genes using BRAKER (Hoff et al., 2019) with multiple RNA-seq libraries (Table S3).

This genome has been deposited to GenBank under the accession JAIUCT000000000.

Differential expression analysis

613

614 Candidate *bicycle* genes from *H. cornu*, *T. ulmi*, and *A. pisum* identified by the classifier
615 were manually re-annotated in APOLLO (Dunn et al., 2019) guided by RNAseq data viewed in
616 IGV (Thorvaldsdóttir et al., 2013). Samples used for analysis are described in Table S3-5.
617 Differential expression analyses were performed as described previously (Korgaonkar et al.,
618 2021) and full analysis scripts are provided at https://doi/figshare_spaceholder.

619

620 *hmmer and BLAST searches*

621

622 The phylogeny of all species studied here was estimated using *Orthofinder* v 2.3.1
623 (Emms and Kelly, 2018) on the complete gene sets predicted by BRAKER for all genomes
624 using the following settings: *-M msa -S diamond -A mafft -T fasttree*. The phylogeny was
625 plotted using *ggtree* v. 2.0.4 in *R*.

626 We searched for *bicycle* homologs in all aphid species and outgroups using Position-
627 Specific Interactive Basic Local Alignment Search Tool (PSI-BLAST) (Altschul, 1997) and
628 *hmmer* (Eddy, 2011). We ran *PSI-BLAST* v. 2.9.0+ using *-max_target_seqs 5* and all other
629 parameters as default. We used a cutoff of $E < 0.01$, Bonferroni corrected for 476 genes used
630 as query searches. We ran profile-based *hmmsearch* v.3.2.1 using all default parameters and
631 cutoff of $E < 0.01$ without multiple testing correction.

632

633 *Selection tests*

634

635 *DnDs* between *H. cornu* and *H. hamamelidis* for all transcripts in the transcriptome was
636 calculated using the *codeml* function from the *PAML* package v4.9j (Yang, 2007). The genome-

wide selection scan was performed using *SweeD-P* v.3.1 (Pavlidis et al., 2013). Details of both analyses can be found in the Methods section of Korgaonkar et al., 2021.

Gene-structure aware sequence alignment

We performed gene structure aware alignment using *prrn5* v 5.2.0 (Gotoh, 2021) with default weighting parameters. We prepared gene-structure-informed extended fasta files that were suitable as input to *prrn5* using the *anno2gsiseq.pl* utility provided at https://github.com/ogotoh/prrn_aln/blob/master/perl/anno2gsiseq.pl. We summarized the results of these multiple sequence alignments by generating histograms with a bin size of 1 to illustrate the fraction of sequences in the alignment that had an intron at each position in the alignment.

To determine whether intron positions were shared between genes more often than expected by chance, we computed the concordance in intron positions resulting from *prrn5* alignment of groups of unrelated genes. We identified paralog groups for the whole *H. cornu* transcriptome using *Orthofinder* v 2.3.3 (Emms and Kelly, 2018) and identified three paralog groups containing at least 10 genes and having at least 10 exons for comparison with *bicycle* genes: *SLC33A1*, *abcG23*, and *nrf-6*. Intron concordance was measured as the correlation coefficient (R) between the number of genes from the test gene family and the *bicycle* gene family containing an intron at each location in the alignment (Figure S6).

Re-annotation of previously sequenced genomes

The *P. venusta* genome is an approximately full-chromosome genome assembly that was kindly provided to us by Yiyuan Li and Nancy Moran (Y. Li et al., 2020) prior to publication.

All other genomes, except for *H. cornu* and *T. ulmi*, were downloaded from NCBI (Table S5). We downloaded RNAseq data from NCBI (Table S4) and predicted coding genes using BRAKER (Hoff et al., 2019) with the same workflow we had used previously that had allowed discovery of *bicycle* genes (Korgaonkar et al., 2021).

Availability of Data and Materials

All new sequence data generated during this study is available at NCBI at the accession numbers provided in Tables S2-4. All analysis scripts, which allow reproduction of all analyses and reproduction of all figures, are provided as Supplementary Material.

Acknowledgements

We thank Andrew Lemire and the whole Quantitative Genomics team at Janelia Research Campus for generating and sequencing the RNA-seq samples, Tom Dolafi for maintaining our Apollo Annotation server, Zari Zavala-Ruiz and the Janelia Visitor Project for supporting CH, Fernando Bazan for recommending the use of RADAR software to detect internal repeats in *megacycle* genes, Gregory Davis for providing samples of *A. pisum*, and Patrick Reilly, Saskia Hogenhout and members of the Stern lab for critical feedback on this work and this manuscript, especially Aishwarya Korgaonkar.

Funding

The authors are employees of Howard Hughes Medical Institute. The funders had no role in the design of the study or in data collection, analysis, and interpretation or in writing of the paper.

Contributions

DLS conceptualized the project, collected aphids, performed dissections, made DNA and most RNA samples, performed initial analyses, and wrote the paper. CH developed the bicycle gene classifier, independently verified all of the computational analyses, and assisted with preparations of figures and manuscript.

Ethics declarations

HHMI has filed a provisional patent, number 63/243,904, for the inventors DLS and CH covering a gene structure, coding sequence-independent method of identifying bicycle genes.

References

Aguiar ERGR, Olmo RP, Paro S, Ferreira FV, de Faria IJ da S, Todjro YMH, Lobo FP, Kroon EG, Meignin C, Gatherer D, Imler J-L, Marques JT. 2015. Sequence-independent characterization of viruses based on the pattern of viral small RNAs produced by the host. *Nucleic Acids Research* **43**:6191–6206. doi:10.1093/nar/gkv587

Altschul S. 1997. Gapped BLAST and PSI-BLAST: a new generation of protein database search programs. *Nucleic Acids Research* **25**:3389–3402. doi:10.1093/nar/25.17.3389

Altschul SF, Gish W, Miller W, Myers EW, Lipman DJ. 1990. Basic local alignment search tool. *Journal of Molecular Biology* **215**:403–410. doi:10.1016/S0022-2836(05)80360-2

Álvarez RA, González-Sierra S, Candelas A, Martinez J-JI. 2013. Histological study of galls induced by aphids on leaves of Ulmus minor : Tetraneura ulmi induces globose galls and Eriosoma ulmi induces pseudogalls. *Arthropod-Plant Interactions* **7**:643–650. doi:10.1007/s11829-013-9278-8

Bazan JF. 1991. Neuropoietic cytokines in the hematopoietic fold. *Neuron* **7**:197–208. doi:10.1016/0896-6273(91)90258-2

Beardsley JW, Gonzalez RH. 1975. The Biology and Ecology of Armored Scales. *Annu Rev Entomol* **20**:47–73. doi:10.1146/annurev.en.20.010175.000403

Betts MJ. 2001. Exon structure conservation despite low sequence similarity: a relic of dramatic events in evolution? *The EMBO Journal* **20**:5354–5360. doi:10.1093/emboj/20.19.5354

Biello R, Singh A, Godfrey CJ, Fernández FF, Mugford ST, Powell G, Hogenhout SA, Mathers TC. 2021. A chromosome-level genome assembly of the woolly apple aphid, *Eriosoma lanigerum* Hausmann (Hemiptera: Aphididae). *Mol Ecol Resour* **21**:316–326. doi:10.1111/1755-0998.13258

Brown NP, Whittaker AJ, Newell WR, Rawlings CJ, Beck S. 1995. Identification and analysis of multigene families by comparison of exon fingerprints. *Journal of Molecular Biology* **249**:342–359. doi:10.1006/jmbi.1995.0301

Burstein M, Wool D, Eshel A. 1994. Sink strength and clone size of sympatric, gall-forming aphids. *European Journal of Entomology* **91**:57–61.

Caillaud CM, Boutin M, Braendle C, Simon JC. 2002. A sex-linked locus controls wing polymorphism in males of the pea aphid, Acyrthosiphon pisum (Harris). *Heredity* **89**:346–352.

Chen W, Hasegawa DK, Kaur N, Kliot A, Pinheiro PV, Luan J, Stensmyr MC, Zheng Y, Liu W, Sun H, Xu Y, Luo Y, Kruse A, Yang X, Kontsedalov S, Lebedev G, Fisher TW, Nelson DR, Hunter WB, Brown JK, Jander G, Cilia M, Douglas AE, Ghanim M, Simmons AM, Wintermantel WM, Ling K-S, Fei Z. 2016. The draft genome of whitefly Bemisia tabaci MEAM1, a global crop pest, provides novel insights into virus transmission, host adaptation, and insecticide resistance. *BMC Biol* **14**:110. doi:10.1186/s12915-016-0321-y

Chen W, Shakir S, Bigham M, Richter A, Fei Z, Jander G. 2019. Genome sequence of the corn leaf aphid (*Rhopalosiphum maidis* Fitch). *GigaScience* **8**. doi:10.1093/gigascience/giz033

Chen Y, Singh A, Kaithakottil GG, Mathers TC, Gravino M, Mugford ST, Oosterhout C van, Swarbreck D, Hogenhout SA. 2020. An aphid RNA transcript migrates systemically within plants and is a virulence factor. *PNAS* **117**:12763–12771. doi:10.1073/pnas.1918410117

745 Coleman AD, Wouters RHM, Mugford ST, Hogenhout SA. 2015. Persistence and
746 transgenerational effect of plant-mediated RNAi in aphids. *Journal of Experimental*
747 *Botany* **66**:541–548. doi:10.1093/jxb/eru450
748 Cook L g., Gullan P j. 2004. The gall-inducing habit has evolved multiple times among the
749 eriococcid scale insects (Sternorrhyncha: Coccoidea: Eriococcidae). *Biological Journal*
750 *of the Linnean Society* **83**:441–452. doi:10.1111/j.1095-8312.2004.00396.x
751 Dixon AFG. 1978. Biology of aphids, Studies in Biology. London: Edward Arnold.
752 Dommel M, Oh J, Huguet-Tapia JC, Guy E, Boulain H, Sugio A, Murugan M, Legeai F, Heck
753 M, Smith CM, White FF. 2020. Big Genes, Small Effectors: Pea Aphid Cassette Effector
754 Families Composed From Miniature Exons. *Front Plant Sci* **11**.
755 doi:10.3389/fpls.2020.01230
756 Dunn NA, Unni DR, Diesh C, Munoz-Torres M, Harris NL, Yao E, Rasche H, Holmes IH, Elsik
757 CG, Lewis SE. 2019. Apollo: Democratizing genome annotation. *PLoS Comput Biol*
758 **15**:e1006790. doi:10.1371/journal.pcbi.1006790
759 Eddy SR. 2011. Accelerated profile HMM searches. *PLoS Computational Biology* **7**.
760 doi:10.1371/journal.pcbi.1002195
761 Eizaguirre C, Lenz TL, Kalbe M, Milinski M. 2012. Rapid and adaptive evolution of MHC genes
762 under parasite selection in experimental vertebrate populations. *Nature Communications*
763 **3**:1–6. doi:10.1038/ncomms1632
764 Elzinga DA, Jander G. 2013. The role of protein effectors in plant-aphid interactions. *Current*
765 *Opinion in Plant Biology* **16**:451–456. doi:10.1016/j.pbi.2013.06.018
766 Emms DM. 2019. OrthoFinder: phylogenetic orthology inference for comparative genomics 14.
767 Emms DM, Kelly S. 2018. STAG: Species Tree Inference from All Genes. *bioRxiv* 1–29.
768 doi:https://doi.org/10.1101/267914
769 Gao Y, Ren R, Peng J, Wang D, Shi X, Zheng L, Zhang Z, Zhu C, Liu Y, Dai L, Zhang D. 2021.
770 The Gustavus Gene Can Regulate the Fecundity of the Green Peach Aphid, Myzus
771 persicae (Sulzer). *Front Physiol* **11**:596392. doi:10.3389/fphys.2020.596392
772 Giron D, Huguet E, Stone GN, Body MJA. 2016. Insect-induced effects on plants and possible
773 effectors used by galling and leaf-mining insects to manipulate their host-plant. *Journal*
774 *of Insect Physiology* **84**:70–89. doi:10.1016/j.jinsphys.2015.12.009
775 Gotoh O. 2021. Cooperation of Spaln and Prrn5 for Construction of Gene-Structure-Aware
776 Multiple Sequence Alignment In: Katoh K, editor. Multiple Sequence Alignment,
777 Methods in Molecular Biology. New York, NY: Springer US. pp. 71–88.
778 doi:10.1007/978-1-0716-1036-7_5
779 Grabherr MG, Haas BJ, Yassour M, Levin JZ, Thompson DA, Amit I, Adiconis X, Fan L,
780 Raychowdhury R, Zeng Q, Chen Z, Mauceli E, Hacohen N, Gnirke A, Rhind N, di Palma
781 F, Birren BW, Nusbaum C, Lindblad-Toh K, Friedman N, Regev A. 2011. Full-length
782 transcriptome assembly from RNA-Seq data without a reference genome. *Nat Biotechnol*
783 **29**:644–652. doi:10.1038/nbt.1883
784 Han J, Lee Y, Yeom K-H, Nam J-W, Heo I, Rhee J-K, Sohn SY, Cho Y, Zhang B-T, Kim VN.
785 2006. Molecular basis for the recognition of primary microRNAs by the Drosha-DGCR8
786 complex. *Cell* **125**:887–901. doi:10.1016/j.cell.2006.03.043
787 Heger A, Holm L. 2000. Rapid automatic detection and alignment of repeats in protein
788 sequences. *Proteins: Structure, Function, and Bioinformatics* **41**:224–237.
789 doi:10.1002/1097-0134(20001101)41:2<224::AID-PROT70>3.0.CO;2-Z

Hoff KJ, Lomsadze A, Borodovsky M, Stanke M. 2019. Whole-genome annotation with BRAKER, Methods in Molecular Biology. doi:10.1007/978-1-4939-9173-0_5

Hogenhout SA, Bos JIB. 2011. Effector proteins that modulate plant-insect interactions. *Current Opinion in Plant Biology* **14**:422–428. doi:10.1016/j.pbi.2011.05.003

Johnson KP, Dietrich CH, Friedrich F, Beutel RG, Wipfler B, Peters RS, Allen JM, Petersen M, Donath A, Walden KKO, Kozlov AM, Podsiadlowski L, Mayer C, Meusemann K, Vasilikopoulos A, Waterhouse RM, Cameron SL, Weirauch C, Swanson DR, Percy DM, Hardy NB, Terry I, Liu S, Zhou X, Misof B, Robertson HM, Yoshizawa K. 2018. Phylogenomics and the evolution of hemipteroid insects. *Proceedings of the National Academy of Sciences* 201815820–201815820. doi:10.1073/pnas.1815820115

Johnson LS, Eddy SR, Portugaly E. 2010. Hidden Markov model speed heuristic and iterative HMM search procedure. *BMC Bioinformatics* **11**. doi:10.1186/1471-2105-11-431

Julca I, Marcet-Houben M, Cruz F, Vargas-Chavez C, Johnston JS, Gómez-Garrido J, Frias L, Corvelo A, Loska D, Cámara F, Gut M, Alioto T, Latorre A, Gabaldón T. 2020. Phylogenomics Identifies an Ancestral Burst of Gene Duplications Predating the Diversification of Aphidomorpha. *Molecular Biology and Evolution* **37**:730–756. doi:10.1093/molbev/msz261

Kohli S, Gulati P, Narang A, Maini J, Shamsudheen KV, Pandey R, Scaria V, Sivasubbu S, Brahmachari V. 2021. Genome and transcriptome analysis of the mealybug Maconellicoccus hirsutus: Correlation with its unique phenotypes. *Genomics* **113**:2483–2494. doi:10.1016/j.ygeno.2021.05.014

Korgaonkar A, Han C, Lemire AL, Siwanowicz I, Bennouna D, Kopec RE, Andolfatto P, Shigenobu S, Stern DL. 2021. A novel family of secreted insect proteins linked to plant gall development. *Current Biology* **31**:1836-1849.e12. doi:10.1016/j.cub.2021.01.104

Le Trionnaire G, Tanguy S, Hudaverdian S, Gleonnec F, Richard G, Cayrol B, Monsion B, Pichon E, Deshoux M, Webster C, Uzest M, Herpin A, Tagu D. 2019. An integrated protocol for targeted mutagenesis with CRISPR-Cas9 system in the pea aphid. *Insect Biochemistry and Molecular Biology* **110**:34–44. doi:10.1016/j.ibmb.2019.04.016

Li M, Tong H, Wang S, Ye W, Li Zicheng, Omar MAA, Ao Y, Ding S, Li Zihao, Wang Y, Yin C, Zhao X, He K, Liu F, Chen X, Mei Y, Walters JR, Jiang M, Li F. 2020. A chromosome-level genome assembly provides new insights into paternal genome elimination in the cotton mealybug *Phenacoccus solenopsis*. *Mol Ecol Resour* **20**:1733–1747. doi:10.1111/1755-0998.13232

Li Y, Park H, Smith TE, Moran NA, Singh N. 2019. Gene Family Evolution in the Pea Aphid Based on Chromosome-level Genome Assembly. *Molecular Biology and Evolution* **36**:2143–2156. doi:10.1093/molbev/msz138

Li Y, Zhang B, Moran NA. 2020. The Aphid X Chromosome Is a Dangerous Place for Functionally Important Genes: Diverse Evolution of Hemipteran Genomes Based on Chromosome-Level Assemblies. *Molecular Biology and Evolution* **37**:2357–2368. doi:10.1093/molbev/msaa095

Loewenstein Y, Raimondo D, Redfern OC, Watson J, Frishman D, Linial M, Orengo C, Thornton J, Tramontano A. 2009. Protein function annotation by homology-based inference. *Genome Biol* **10**:207. doi:10.1186/gb-2009-10-2-207

Madeira F, Park Y mi, Lee J, Buso N, Gur T, Madhusoodanan N, Basutkar P, Tivey ARN, Potter SC, Finn RD, Lopez R. 2019. The EMBL-EBI search and sequence analysis tools APIs in 2019. *Nucleic Acids Research* **47**:W636–W641. doi:10.1093/nar/gkz268

Mani MS. 1964. Ecology of Plant Galls. The Hague, The Netherlands: Springer-Science+Business Media, B.V. doi:10.2307/3756723

Mathers TC, Chen Y, Kaithakottil G, Legeai F, Mugford ST, Baa-Puyoulet P, Bretaudeau A, Clavijo B, Colella S, Collin O, Dalmay T, Derrien T, Feng H, Gabaldón T, Jordan A, Julca I, Kettles GJ, Kowitwanich K, Lavenier D, Lenzi P, Lopez-Gomollon S, Loska D, Mapleson D, Maumus F, Moxon S, Price DRGG, Sugio A, Munster MV, Uzest M, Waite D, Jander G, Tagu D, Wilson ACCC, van Munster M, Uzest M, Waite D, Jander G, Tagu D, Wilson ACCC, van Oosterhout C, Swarbreck D, Hogenhout SA. 2017. Rapid transcriptional plasticity of duplicated gene clusters enables a clonally reproducing aphid to colonise diverse plant species. *Genome Biology* **18**:1–20. doi:10.1186/s13059-016-1145-3

Mathers TC, Mugford ST, Hogenhout SA, Tripathi L. 2020. Genome Sequence of the Banana Aphid, *Pentalonia nigronervosa* Coquerel (Hemiptera: Aphididae) and Its Symbionts. *G3 Genes|Genomes|Genetics* **10**:4315–4321. doi:10.1534/g3.120.401358

Mathers TC, Wouters RHM, Mugford ST, Swarbreck D, van Oosterhout C, Hogenhout SA. 2021. Chromosome-Scale Genome Assemblies of Aphids Reveal Extensively Rearranged Autosomes and Long-Term Conservation of the X Chromosome. *Molecular Biology and Evolution* **38**:856–875. doi:10.1093/molbev/msaa246

Mutti NS, Louis J, Pappan LK, Pappan K, Begum K, Chen MS, Park Y, Dittmer N, Marshall J, Reese JC, Reeck GR. 2008. A protein from the salivary glands of the pea aphid, Acyrthosiphon pisum, is essential in feeding on a host plant. *Proceedings of the National Academy of Sciences of the United States of America* **105**:9965–9969. doi:10.1073/pnas.0708958105

Mutti NS, Park Y, Reeck. 2006. RNAi knockdown of a salivary transcript leading to lethality in the pea aphid, Acyrthosiphon pisum. *Journal of Insect Science* **6**.

Nicholson SJ, Nickerson ML, Dean M, Song Y, Hoyt PR, Rhee H, Kim C, Puterka GJ. 2015. The genome of Diuraphis noxia, a global aphid pest of small grains. *BMC Genomics* **16**:429. doi:10.1186/s12864-015-1525-1

Nishimura O, Hara Y, Kuraku S. 2017. GVolante for standardizing completeness assessment of genome and transcriptome assemblies. *Bioinformatics* **33**:3635–3637. doi:10.1093/bioinformatics/btx445

Niu J, Yang W, Tian Y, Fan J, Ye C, Shang F, Ding B, Zhang J, An X, Yang L, Chang T, Christiaens O, Smagghe G, Wang J. 2019. Topical dsRNA delivery induces gene silencing and mortality in the pea aphid. *Pest Manag Sci* **75**:2873–2881. doi:10.1002/ps.5457

Nováková E, Hypša V, Klein J, Foottit RG, von Dohlen CD, Moran NA. 2013. Reconstructing the phylogeny of aphids (Hemiptera: Aphididae) using DNA of the obligate symbiont Buchnera aphidicola. *Molecular Phylogenetics and Evolution* **68**:42–54. doi:10.1016/j.ympev.2013.03.016

Parr T. 1940. Asterolecanium Variolosum Ratzeburg, A Gall-Forming Coccid, and its Effect Upon the Host Trees. *YALE SCHOOL OF THE ENVIRONMENT BULLETIN SERIES* 90.

Paterson S, Vogwill T, Buckling A, Benmayor R, Spiers AJ, Thomson NR, Quail M, Smith F, Walker D, Libberton B, Fenton A, Hall N, Brockhurst MA. 2010. Antagonistic coevolution accelerates molecular evolution. *Nature* **464**:275–278. doi:10.1038/nature08798

Pavlidis P, Zˇivkovic D, Stamatakis A, Alachiotis N. 2013. SweeD: Likelihood-Based Detection of Selective Sweeps in Thousands of Genomes. *Molecular Biology & Evolution* **30**:2224–2234.

Pitino M, Coleman AD, Maffei ME, Ridout CJ, Hogenhout SA. 2011. Silencing of Aphid Genes by dsRNA Feeding from Plants. *PLOS ONE* **6**:e25709. doi:10.1371/journal.pone.0025709

Quan Q, Hu X, Pan B, Zeng B, Wu N, Fang G, Cao Y, Chen X, Li X, Huang Y, Zhan S. 2019. Draft genome of the cotton aphid Aphis gossypii. *Insect Biochemistry and Molecular Biology* **105**:25–32. doi:10.1016/j.ibmb.2018.12.007

Richards S, Gibbs RA, Gerardo NM, Moran N, Nakabachi A, Stern D, Tagu D, Wilson ACC, Muzny D, Kovar C, Cree A, Chacko J, Chandrabose MN, Dao MD, Dinh HH, Gabisi RA, Hines S, Hume J, Jhangian SN, Joshi V, Lewis LR, Liu YS, Lopez J, Morgan MB, Nguyen NB, Okwuonu GO, Ruiz SJ, Santibanez J, Wright RA, Fowler GR, Hitchens ME, Lozado RJ, Moen C, Steffen D, Warren JT, Zhang J, Nazareth LV, Chavez D, Davis C, Lee SL, Patel BM, Pu LL, Bell SN, Johnson AJ, Vattathil S, Williams RL, Shigenobu S, Dang PM, Morioka M, Fukatsu T, Kudo T, Miyagishima SY, Jiang H, Worley KC, Legeai F, Gauthier JP, Collin O, Zhang L, Chen HC, Ermolaeva O, Hlavina W, Kapustin Y, Kiryutin B, Kitts P, Maglott D, Murphy T, Pruitt K, Sapojnikov V, Souvorov A, Thibaud-Nissen F, Câmara F, Guigó R, Stanke M, Solovyev V, Kosarev P, Gilbert D, Gabaldón T, Huerta-Cepas J, Marcet-Houben M, Pignatelli M, Moya A, Rispe C, Ollivier M, Quesneville H, Permal E, Llorens C, Futami R, Hedges D, Robertson HM, Alioto T, Mariotti M, Nikoh N, McCutcheon JP, Burke G, Kamins A, Latorre A, Ashton P, Calevro F, Charles H, Colella S, Douglas AE, Jander G, Jones DH, Febvay G, Kamphuis LG, Kushlan PF, Macdonald S, Ramsey J, Schwartz J, Seah S, Thomas G, Vellozo A, Cass B, Degnan P, Hurwitz B, Leonardo T, Koga R, Altincicek B, Anselme C, Atamian H, Barribeau SM, De Vos M, Duncan EJ, Evans J, Ghanim M, Heddi A, Kaloshian I, Vincent-Monegat C, Parker BJ, Pérez-Brocal V, Rahbé Y, Spragg CJ, Tamames J, Tamarit D, Tamborindeguy C, Vilcinskas A, Bickel RD, Brisson JA, Butts T, Chang CC, Christiaens O, Davis GK, Duncan EJ, Ferrier D, Iga M, Janssen R, Lu HL, McGregor A, Miura T, Smagghe G, Smith J, Van Der Zee M, Velarde R, Wilson M, Dearden P, Edwards OR, Gordon K, Hilgarth RS, Rider SD, Srinivasan D, Walsh TK, Ishikawa A, Jaubert-Possamai S, Fenton B, Huang W, Rizk G, Lavenier D, Nicolas J, Smadja C, Zhou JJ, Vieira FG, He XL, Liu R, Rozas J, Field LM, Campbell P, Carolan JC, Fitzroy CIJ, Reardon KT, Reeck GR, Singh K, Wilkinson TL, Huybrechts J, Abdel-Latief M, Robichon A, Veenstra JA, Hauser F, Cazzamali G, Schneider M, Williamson MMS, Stafflinger E, Hansen KK, Grimmelikhuijzen CJP, Price DRG, Caillaud M, Van Fleet E, Ren Q, Gatehouse JA, Brault V, Monsion B, Diaz J, Hunnicutt L, Ju HJ, Pechuan X, Aguilar J, Cortés T, Ortiz-Rivas B, Martínez-Torres D, Dombrovsky A, Dale RP, Davies TGE, Williamson MMS, Jones A, Sattelle D, Williamson S, Wolstenholme A, Cottret L, Sagot MF, Heckel DG, Hunter W, Consortium TIAG. 2010. Genome Sequence of the Pea Aphid Acyrthosiphon pisum. *PLoS Biol* **8**:e1000313–e1000313. doi:10.1371/journal.pbio.1000313

Rispe C, Legeai F, Nabity PD, Fernández R, Arora AK, Baa-Puyoulet P, Banfill CR, Bao L, Barberà M, Bouallègue M, Bretaudeau A, Brisson JA, Calevro F, Capy P, Catrice O, Chertemps T, Couture C, Delière L, Douglas AE, Dufault-Thompson K, Escuer P, Feng H, Forneck A, Gabaldón T, Guigó R, Hilliou F, Hinojosa-Alvarez S, Hsiao Y,

927 Hudaverdian S, Jacquin-Joly E, James EB, Johnston S, Joubard B, Le Goff G, Le
928 Trionnaire G, Librado P, Liu S, Lombaert E, Lu H, Maïbèche M, Makni M, Marcet-
929 Houben M, Martínez-Torres D, Meslin C, Montagné N, Moran NA, Papura D, Parisot N,
930 Rahbé Y, Lopes MR, Ripoll-Cladellas A, Robin S, Roques C, Roux P, Rozas J, Sánchez-
931 Gracia A, Sánchez-Herrero JF, Santesmasses D, Scatoni I, Serre R-F, Tang M, Tian W,
932 Umina PA, van Munster M, Vincent-Monégat C, Wemmer J, Wilson ACC, Zhang Y,
933 Zhao C, Zhao J, Zhao S, Zhou X, Delmotte F, Tagu D. 2020. The genome sequence of
934 the grape phylloxera provides insights into the evolution, adaptation, and invasion routes
935 of an iconic pest. *BMC Biol* **18**:90. doi:10.1186/s12915-020-00820-5
936 Rodriguez PA, Escudero-Martinez C, Bos JIB. 2017. An Aphid Effector Targets Trafficking
937 Protein VPS52 in a Host-Specific Manner to Promote Virulence. *Plant Physiol*
938 **173**:1892–1903. doi:10.1104/pp.16.01458
939 Rokas A, Holland PWH. 2000. Rare genomic changes as a tool for phylogenetics. *Trends in*
940 *Ecology and Evolution* **15**:454–459.
941 Rokas A, Kathirithamby J, Holland PWH. 1999. Intron insertion as a phylogenetic character: the
942 engrailed homeobox of Strepsiptera does not indicate affinity with Diptera. *Insect*
943 *Molecular Biology* **8**:527–530.
944 Roy SW, Gilbert W. 2005. Rates of intron loss and gain: Implications for early eukaryotic
945 evolution. *Proc Natl Acad Sci U S A* **102**:5773–5778. doi:10.1073/pnas.0500383102
946 Ruvinsky A, Watson C. 2007. Intron Phase Patterns in Genes: Preservation and Evolutionary
947 Changes. *TOEVOLJ* **1**:1–14. doi:10.2174/1874404400701010001
948 Saha S, Hosmani PS, Villalobos-Ayala K, Miller S, Shippy T, Flores M, Rosendale A, Cordola
949 C, Bell T, Mann H, DeAvila G, DeAvila D, Moore Z, Buller K, Ciolkevich K, Nandyal
950 S, Mahoney R, Van Voorhis J, Dunlevy M, Farrow D, Hunter D, Morgan T, Shore K,
951 Guzman V, Izsak A, Dixon DE, Cridge A, Cano L, Cao X, Jiang H, Leng N, Johnson S,
952 Cantarel BL, Richards S, English A, Shatters RG, Childers C, Chen M-J, Hunter W, Cilia
953 M, Mueller LA, Munoz-Torres M, Nelson D, Poelchau MF, Benoit JB, Wiersma-Koch
954 H, D'Elia T, Brown SJ. 2017. Improved annotation of the insect vector of citrus greening
955 disease: biocuration by a diverse genomics community. *Database* **2017**.
956 doi:10.1093/database/bax032
957 Schaible G, Lee DJ, Kim CS, Schaible G, Garrett L, Lubowski R. 2008. Economic Impacts of
958 the U. S. Soybean Aphid Infestation : A Multi-Regional Competitive Dynamic Analysis.
959 *Agricultural and Resource Economics Review* **37**:227–242.
960 doi:10.1017/S1068280500003026
961 Shakesby AJ, Wallace IS, Isaacs HV, Pritchard J, Roberts DM, Douglas AE. 2009. A water-
962 specific aquaporin involved in aphid osmoregulation. *Insect Biochemistry and Molecular*
963 *Biology* **39**:1–10. doi:10.1016/j.ibmb.2008.08.008
964 Shorthouse JD, Wool D, Raman A. 2005. Gall-inducing insects - Nature's most sophisticated
965 herbivores. *Basic and Applied Ecology* **6**:407–411. doi:10.1016/j.baae.2005.07.001
966 Telford MJ, Copley RR. 2011. Improving animal phylogenies with genomic data. *Trends in*
967 *Genetics* **27**:186–195. doi:10.1016/j.tig.2011.02.003
968 Thorvaldsdóttir H, Robinson JT, Mesirov JP. 2013. Integrative Genomics Viewer (IGV): High-
969 performance genomics data visualization and exploration. *Briefings in Bioinformatics*
970 **14**:178–192. doi:10.1093/bib/bbs017

Vakirlis N, Carvunis A-R, McLysaght A. 2020. Synteny-based analyses indicate that sequence divergence is not the main source of orphan genes. *eLife* **9**:e53500. doi:10.7554/eLife.53500

Vellichirammal NN, Gupta P, Hall TA, Brisson JA. 2017. Ecdysone signaling underlies the pea aphid transgenerational wing polyphenism. *Proceedings of the National Academy of Sciences of the United States of America* **114**:1419–1423. doi:10.1073/pnas.1617640114

Venkatesh B, Ning Y, Brenner S. 1999. Late changes in spliceosomal introns define clades in vertebrate evolution. *Proceedings of the National Academy of Sciences* **96**:10267–10271. doi:10.1073/pnas.96.18.10267

von Dohlen and N. A. Moran CD. 1995. Molecular phylogeny of the Homoptera: a paraphyletic taxon. *J Mol Evol* **41**:211–223.

Weisenfeld NI, Kumar V, Shah P, Church DM, Jaffe DB. 2017. Direct determination of diploid genome sequences. *Genome research* **27**:757–767. doi:10.1101/gr.235812.118

Weisman CM, Murray AW, Eddy SR. 2020. Many, but not all, lineage-specific genes can be explained by homology detection failure. *PLoS Biol* **18**:e3000862. doi:10.1371/journal.pbio.3000862

Will T, Tjallingii WF, Thönnessen A, van Bel AJE. 2007. Molecular sabotage of plant defense by aphid saliva. *Proceedings of the National Academy of Sciences of the United States of America* **104**:10536–10541. doi:10.1073/pnas.0703535104

Will T, Vilcinskas A. 2015. The structural sheath protein of aphids is required for phloem feeding. *Insect Biochemistry and Molecular Biology* **57**:34–40. doi:10.1016/j.ibmb.2014.12.005

Xie W, He C, Fei Z, Zhang Y. 2020. Chromosome-level genome assembly of the greenhouse whitefly (Trialeurodes vaporariorum Westwood). *Molecular Ecology Resources* **20**:995–1006. doi:10.1111/1755-0998.13159

Xue J, Zhou X, Zhang C-X, Yu L-L, Fan H-W, Wang Z, Xu H-J, Xi Y, Zhu Z-R, Zhou W-W, Pan P-L, Li B-L, Colbourne JK, Noda H, Suetsugu Y, Kobayashi T, Zheng Y, Liu S, Zhang R, Liu Y, Luo Y-D, Fang D-M, Chen Y, Zhan D-L, Lv X-D, Cai Y, Wang Z-B, Huang H-J, Cheng R-L, Zhang X-C, Lou Y-H, Yu B, Zhuo J-C, Ye Y-X, Zhang W-Q, Shen Z-C, Yang H-M, Wang Jian, Wang Jun, Bao Y-Y, Cheng J-A. 2014. Genomes of the rice pest brown planthopper and its endosymbionts reveal complex complementary contributions for host adaptation. *Genome Biol* **15**:521. doi:10.1186/s13059-014-0521-0

Yang P, Yu S, Hao J, Liu W, Zhao Z, Zhu Z, Sun T, Wang X, Song Q. 2019. Genome sequence of the Chinese white wax scale insect Ericerus pela: the first draft genome for the Coccidae family of scale insects. *GigaScience* **8**:giz113. doi:10.1093/gigascience/giz113

Yang Z. 2007. PAML 4: Phylogenetic Analysis by Maximum Likelihood. *Molecular Biology and Evolution* **24**:1586–1591. doi:10.1093/molbev/msm088

Zhang B, Ma C, Edwards O, Fuller S, Kang L. 2014. The mitochondrial genome of the Russian wheat aphid Diuraphis noxia: Large repetitive sequences between trnE and trnF in aphids. *Gene* **533**:253–260. doi:10.1016/j.gene.2013.09.064

Zhu J, Jiang F, Wang X, Yang P, Bao Y, Zhao W, Wang W, Lu H, Wang Q, Cui N, Li J, Chen X, Luo L, Yu J, Kang L, Cui F. 2017. Genome sequence of the small brown planthopper, Laodelphax striatellus. *GigaScience* **6**. doi:10.1093/gigascience/gix109

1016 **Figure Legends**

1017

1018 Figure 1. The gene-structure based classifier detects *bicycle* genes in genomes of aphids,
1019 phylloxerids, and coccids. A whole-proteome phylogeny of the species studied is shown on
1020 the left. Family membership is shown in color beside the species names. The number of
1021 candidate *bicycle* homologs detected by *BLAST*, *hmmer*, and the gene-structure based
1022 classifier is shown to the right of the phylogeny. The number of candidate *bicycle* homologs
1023 detected by profile *hmmer* starting with the *bicycle* homologs identified by the gene-structure
1024 based classifier within each species is shown in the far right column.

1025

1026 Figure 2. The gene-structure based classifier identifies additional CYC and non-CYC motif
1027 containing genes in the *H. cornu* genome that may contribute to the effector protein repertoire
1028 of multiple stages of the *H. cornu* life cycle.

1029 (A) Hierarchical clustering of candidate *H. cornu bicycle* homologs detected by the gene-
1030 structure based on amino-acid sequence similarity measure reveals two clusters of
1031 genes with similar sequences. Some of the genes in Cluster 1 appear to have some
1032 sequence similarity to Cluster 2 genes.

1033 (B) Genes in Cluster 1 encode proteins with N-terminal signal sequences and weak
1034 similarity to *bicycle* genes.

1035 (C) Genes in Cluster 2 encode proteins with sequence similarity to the previously described
1036 *bicycle* genes.

1037 (D) Diagram of life cycle of *H. cornu*. Individuals from different generations exhibit
1038 phenotypes that are specialized for each stage of the complex life cycle. The fundatrix
1039 (G1) is the only generation that induces a gall.

1040 (E) A volcano plot of the strength of evidence for differential expression (-log10(P value))
1041 versus the fold-change differential expression of salivary glands isolated from
1042 fundatrices versus sexuals reveals that some of the Cluster1 (black) and 2 (orange)
1043 genes identified by the gene structure based classifier are as strongly enriched in
1044 fundatrix salivary glands as the originally described *bicycle* genes (blue). In addition,
1045 several Cluster 1 and 2 genes are more strongly enriched in salivary glands of sexuals.
1046 (F-G) Plots of gene expression levels for Cluster 1 (F) and 2 (G) genes across four
1047 generations of the life cycle reveals that while most *bicycle* homologs are most strongly
1048 expressed in fundatrix salivary glands (e.g. purple lines), some are weakly expressed in
1049 fundatrix salivary glands and then strongly expressed in salivary glands of individuals
1050 from other stages of the life cycle (e.g. red lines).
1051
1052 Figure 3. *H. cornu bicycle* genes belong to four major categories, *unicycle, bicycle, tricycle,*
1053 and *tetracycle* genes
1054 (A) The originally identified *bicycle* genes encode proteins that exhibit a wide size range,
1055 with representatives of approximately four size classes, indicated by the vertical dotted
1056 blue lines.
1057 (B-E) Logo plots of the proteins from each of the four size classes of Bicycle proteins
1058 identifies Unicycle (B), Bicycle (C), Tricycle (D), and Tetracycle (E) proteins. The CYC
1059 motifs in each protein are identified by thick black lines below each Logo plot.
1060
1061 Figure 4. The *T. ulmi bicycle* homologs detected by the gene-structure based classifier display
1062 CYC motifs and highly divergent protein sequences.
1063 (A) Hierarchical clustering of candidate *T. ulmi bicycle* homologs based on amino-acid
1064 sequence similarity measure reveals four clusters of genes.

1065 (B-E) The four clusters of *T. ulmi bicycle* homologs display two (B, C) or one (D) CYC motif,
1066 or no clear CYC motifs (E). The cluster identities are indicated in each subplot.
1067 (A) Volcano plot of genes differentially expressed in fundatrix salivary glands versus
1068 carcass with *bicycle* genes labelled. Most of the *T. ulmi* candidate *bicycle* homologs are
1069 strongly over-expressed in the fundatrix salivary glands.
1070
1071 Figure 5. *A. pisum bicycle* homologs contain a single CYC motif and are strongly enriched in
1072 salivary glands.
1073 (A) Logo plot of *A. pisum bicycle* homologs detected by gene-structure based classifier.
1074 Most *A. pisum* homologs contain a single CYC motif.
1075 (B) Volcano plot of differential expression between salivary glands and carcass reveals that
1076 *A. pisum bicycle* homologs are strongly over-expressed in salivary glands.
1077
1078 Figure 6. *Megacycle* genes have a repeating protein structure and are overexpressed in
1079 salivary glands of multiple aphid species.
1080 (A) Gene structure of the *M. sacchari megacycle* gene (*g20694*). The gene includes 118
1081 exons encoded in approximately 100 kbp of DNA. The protein is 2092 AA long.
1082 (B) Rapid Automatic Detection and Alignment of Repeats (RADAR) analysis of the
1083 *M. sacchari megacycle* gene provides evidence for 15 repeating units within the
1084 protein encoded by *g20694*. Multiple sequence alignment of these repeat units
1085 (not using information on gene structure) reveals that many introns, marked in
1086 green, are located in identical or similar positions in the aligned sub-sequences.
1087 A logo plot of the aligned repeated sequences is shown above the alignment.

There is no obvious evidence for CYC motifs, although the motif is approximately the same length as the proteins encoded by many *bicycle* genes.

(C-E) Volcano plots of differential expression between salivary glands and carcasses for three species, *H. cornu* (C), *T. ulmi* (D), and *A. pisum* (E), reveals that *megacycle* genes (black dots) are strongly over-expressed in salivary glands of all three species. *Bicycle* genes are marked as light blue dots.

Supplementary Figures

Figure S1. Salient features of gene structure of *H. cornu* bicycle genes.

(A-B) Almost all internal exons of *bicycle* genes are of phase 2 (A), whereas the majority of internal exons of other genes in the *H. cornu* genome are of phase 0 (B).

(C-D) *Bicycle* genes have a wide range of exon numbers, with a distribution (C) different from non-*bicycle* genes (D).

(E-F) The total length of Bicycle proteins is better predicted by the number of exons in the gene (E) than by the length of the first and last exon (F).

Figure S2. Performance of a gene-structure based classifier of *bicycle* genes.

(A) Precision versus recall curves for replicate training runs of the classifier using 100 different subsets of the training data. The curves across all subsets are very similar, indicating that the classifier was not unduly influenced by a specific subset of the data.

(B) Histogram of the number of transcripts with a particular classifier response shows a bimodal distribution. The vast majority of genes (>10,000) had a response close to 0. A threshold of 0.72 was chosen at a precision to recall ratio of 1.

(C) Precision (the proportion of true positives among both true and false positives) versus recall (the proportion of true positives among true positives and false negatives) for the model trained on 476 previously identified *H. cornu bicycle* genes. Differently colored dots represent the precision to recall ratio for different probability cutoffs of the model, shown in panel (D).

(D) The ratio of precision to recall for different cutoffs. Precision approximately equals recall (P/R = 1) at a cutoff of 0.72.

(E) Precision and recall values for models where one variable at a time was removed from the model. Removal of the number of exons with mode2 had the largest decrement on performance, but all models performed well.

(F) Precision and recall values for models where only one predictor variable was included in the model. Exon mean length had the best predictive value on its own, but no single variable performed as well as inclusion of all variables.

(G) Correlation amongst predictor variables for all of the original 476 *bicycle* genes. Most variables are not strongly correlated.

(H) First two principal components of principal component analysis of values for the predictor variables for all of the original 476 *bicycle* genes provides further support that variables are not strongly correlated.

(I) Percent variance explained for the eight principal components of a principal component analysis for the predictor variables for all of the original 476 *bicycle* genes.

Figure S3. Plots of exon number per gene vs median exon size for all species studied. Phylogeny for all species is shown on left and is identical to phylogeny in Figure 1. *Bicycle* genes tend to have many small exons. Red = bicycle classifier, blue = other genes.

1136

1137 Figure S4. Newly identified candidate *bicycle* genes in *H. cornu* exhibit signatures of strong
1138 and recent positive selection.

1139 (A-C) d_N/d_S ratio for the 476 original *bicycle* genes (A), the newly identified putative *bicycle*
1140 genes (B) and the non-*bicycle* genomic background (C) between *H. cornu* and *H.*
1141 *hamamelidis*. Both the original *bicycle* genes and the newly putative *bicycle* genes
1142 show an excess of genes with a ratio of d_N/d_S above 1 compared to the background.
1143 Dashed vertical line indicates d_N/d_S = 1.

1144 (D) Median distance to the closest sweep signal for original *bicycle* genes (red dashed line)
1145 and classifier newly identified putative *bicycle* genes (blue dashed line). Histogram
1146 shows median distance to closest sweep signal for 1000 permutations of gene labels.
1147 The original *bicycle* genes and the new putative *bicycle* genes are both closer to sweep
1148 signals than expected by chance.

1149

1150 Figure S5. Gene-structure aware alignments reveal extensive conservation of intron locations
1151 between the originally-defined *bicycle* genes and putative *bicycle* homologs identified by the
1152 gene-structure based classifier.

1153 (A-D) Predicted proteins encoded by the original or newly identified bicycle homologs were
1154 divided by sequence length into Unicycle (A), Bicycle (B), Tricycle (C), or Tetracycle (D)
1155 proteins and aligned using gene-structure aware alignment. The frequency of introns at
1156 each location in the alignment is plotted for the original (orange) and newly defined
1157 (cyan) *bicycle* homologs and positions without introns were excluded from the plot.
1158 Intron positions are therefore relative to each other and do not indicate absolute
1159 position in the proteins or the alignments. Coincidence of intron positions is shown by
1160 purple bars. Original *bicycle* homologs were randomly down-sampled to 20 genes to

match the number of newly identified *bicycle* homologs to improve overall alignment accuracy (B).

Figure S6. Testing intron concordance. To determine whether concordant introns were found more often than expected by chance alignment of unrelated genes, gene-structure aware alignment was performed between a subset of the original *bicycle* genes and genes from three gene families containing at least 10 genes with at least 10 exons each: *SLC33A1*, *abcG23*, and *nrf-6*. Intron concordance was measured as the correlation coefficient between the number of genes exhibiting an intron in the test gene family versus the original *bicycle* gene family.

(A) Example of gene-structure aware alignment of 23 genes from *SLC33A1* (blue) and 23 original *bicycle* gene (orange) families. One intron was found frequently in both gene families (purple), a pattern observed in most alignments and likely reflects an artifact of the gene-structure aware alignment algorithm.

(B) Example of gene-structure aware alignment of 20 candidate *H. cornu bicycle* genes identified by the classifier (blue) and 20 original *bicycle* genes (orange). Many introns are found in both groups (purple).

(C-D) Examples of quantification of intron concordance, measured as the correlation between the number of genes with an intron at each location in the alignment in the test gene family versus the original *bicycle* genes. For a comparison of the unrelated gene families *SLC33A1* and original *bicycle* (C), the correlation was close to 0. For a comparison of candidate *bicycle* genes versus the original *bicycle* genes, the correlation was high and positive (D).

(E) Intron concordance, measured as the correlation coefficient (*R*) of the number of genes sharing intron locations in gene-structure aware alignments, of repeated re-samplings of unrelated genes families generated a null distribution of expected *R* values for

unrelated genes (*SLC33A1*, *abcG23*, and *nrf-6* versus original *bicycle* genes in red, green and blue histograms, respectively). *R* values for all comparisons of candidate *bicycle* genes found by the classifier and the original *bicycle* genes were all positive and much higher than any of the *R* values resulting from alignment of unrelated gene families, indicating that more introns are shared between genes in these gene-structure aware alignments than expected between unrelated gene families by chance ($P < 0.01$).

Figure S7. *Tetraneura ulmi* life cycle and additional features of *T. ulmi bicycle* genes.

(A) Photo of mature galls of *T. ulmi* on leaf of *Ulmus americana* collected at Janelia Research Campus, Ashburn, VA, USA.

(B) Diagram of life cycle of *T. ulmi*. Samples for differential expression analysis were collected from generations G1 and G2.

(C) The *T. ulmi* putative bicycle homologs from Clusters 1 and 4, with and without CYC motifs, respectively, share multiple intron positions. Proteins from the two classes of genes were aligned using gene-structure aware alignment and the frequency of introns at each location in the alignment was plotted in different colors for the two classes of genes and positions without introns were excluded from the plot. Intron positions are therefore relative to each other and do not indicate absolute position in the proteins or the alignments. Sites of coincident introns are indicated in purple.

Figure S8. The *A. pisum* putative *bicycle* homologs share multiple intron positions with *H. cornu bicycle* genes. Proteins were aligned using gene-structure aware alignment and the frequency of introns at each location in the alignment was plotted in different colors for the two classes of genes and positions without introns were excluded from the plot. Intron positions

are therefore relative to each other and do not indicate absolute position in the proteins or the alignments. Sites of coincident introns are indicated in purple.

Figure S9. Features of *bicycle* homologs detected in aphid species.

(A) A plot of the number of *bicycle* homologs detected by the gene-structure based classifier versus genome N50, a measure of genome assembly quality, shows no significant relationship between these variables (R^2 = 0.09, F = 1.4, P = 0.26).

(B-E) Logo plots of putative *bicycle* homologs detected in four aphid species, *M. persicae* (B), *P. nigronervosa* (C), *R. maidis* (D), and *C. cedri* (E) reveals that they all contain CYC motifs. The *M. persicae* and *P nigronervosa* genes are primarily *unicycles*, the *R. maidis* genes are primarily *bicycles*, and the *C. cedri* genes are primarily *tetracycles*.

Figure S10. Features of *bicycle* homologs detected in outgroups to aphids.

(A-C) Logo plots of proteins encoded by putative *bicycle* homologs detected in *D. vitilifoliae* (A), *M. hirsutus* (B), and *P. solenopsis* (C). The logo plots from these putative homologs show no obvious CYC motifs.

(D-F) Gene-structure aware alignments reveal that multiple introns are shared between these highly divergent putative *bicycle* homologs and *H. cornu bicycle* genes. Positions in alignments without introns were excluded from the plot. Intron positions are therefore relative to each other and do not indicate absolute position in the proteins or the alignments. Sites of coincident introns are indicated in purple.

Figure S11. *Megacycle* genes share intron locations with *bicycle* genes and are found in many aphid species.

(A) Gene-structure aware alignments reveal that multiple introns are shared between *megacycle* genes and *H. cornu bicycle* genes. Positions in alignments without introns were excluded from the plot. Intron positions are therefore relative to each other and do not indicate absolute position in the proteins or the alignments. Shared introns are shown in purple.

(B) Maximum likelihood phylogeny of the protein sequences encoded by *megacycle* genes found in aphid species. *Megacycle* genes were not detected outside of aphids. The phylogeny has a topology similar to the aphid portion of the whole-proteome phylogeny shown in Figure 1. Only one *megacycle* gene was detected in most aphid species, but three paralogs were detected in *C. cedri* and *T. ulmi*. Values at nodes are bootstrap support values. Scale bar is 0.1 substitution per residue.

Supplementary Tables

Table S1. Many microexon genes producing secreted putative effector proteins in *A. pisum* detected by mass spectrometry of secreted proteins (Dommel et al., 2020) are identified as *bicycle* genes by the classifier.

Gene Name (Dommel)	Transcript ID	Gene Locus	Best hit Augustus gene	Peptide sequence	*bicycle* gene according to classifier	Notes
KQY1a, b	NM_001162442, AK339882	LOC100158789	g118916	MIFFKQYSMMITFIVIAVWVMPAITSE	Yes	
KQY2a, b	AK342599 & AK342927	LOC100302371 & LOC100302371	g2591	MVFYKQYLLTITCIVITAWVIPTSA	Yes	
KQY3	AK341661	LOC100301916	g48042	MVFFKQYLITLTCIVISVWITPVNT	Yes	
KQY4a, b, c, d	AK342948, AK342242, AK342690, AK342678	LOC100302370	g139706	MIFFKQYLIILTFIVIAVLVMPVTP	Yes	
KQY5a, b	AK342406, AK342378	LOC100302375, LOC100302376	g108486a	MVFFKQYLLTLTCIVIVVQVMPASA	Yes	
KQY6	AK340126	LOC100302481	g119690 and g3762	MIFFKQYLIMLTFIIIAVWVMPANT	Yes	
KQY7	AK340563	LOC100302485	g103944	MSFFKQYLTLTFIVISVWNMSEA	Yes	
KQY8	AK342473	LOC100302439	g123349	MVFFKQFLITLTVIIITEA	?	

KQY9	AK342683	LOC100302403	No close matches	MVFFKLYLLTLTCIVIAVWVMPVSA	No	Closest match, 76% identity to g2591
KQY10	AK342808	LOC100302381	g39312	MFNVLIILSLISYTFEPSYTLYKFKMVFFKQDLLMLTCITIAVWIMPPSASTN	Yes	
KQY11	AK340121	LOC100302480	g144677	MVFFRQFLITLSVILITEA	No	
KQYMp	XM_022322515	LOC111039170	g115805	MHFFKHYLIVLTYIVISFWFMPSASL	Yes	Myzus persicae
KHI1a, b	AK339863, AK339862	LOC100159750	g119277	MFKHIIVLVLCFMAYFVGNLDA	Yes	85% identical
KHI2a, b, c	AK341162, AK341161, AK342769	LOC100302383	g101192	MDKHIIMLALCLMVYIIGNIDA	Yes	
KHI3a, b	AK340197, AK342603	LOC100166702	g134738	MLKHIIVLALYLMAYIIGNIDA	Yes	
KHI4	AK341077	LOC100570519	g141770	MLKHILLALCFMAYIIENIG	Yes	
KHI5	AK341390	LOC100534636	?	MLKHILLALCFMAYIIENIGA		g141770 closest match, but no match to terminal A.
KHI6	AK340760	LOC100571631	g121945	MLKHIIVLVLCFMPYIIG	Yes	94% identical
C002Ap	XM_001948323	LOC100167863	g50444	MGSYKLYVAVMAIAIAVVQEVRC	No	2 exon gene; not searched by classifier

Table S2—Details of *Tetraneura ulmi* sample, sequence files, and SRA accession numbers for genome sequencing. JRC refers to Janelia Research Campus, Ashburn VA, USA. These sequences can be found under the SRA BioProject PRJNA759586.

Collection Location	Species	Library Prep Method	Sequencing Method	# Read pairs	Accession #
JRC	*Tetraneura ulmi*	10X Chromium	Illumina PE151	441,975,717	SRR15704183

Table S3 - Details of biological samples, sequence files, and SRA accession numbers for *Tetraneua ulmi* RNA-sequencing. JRC refers to Janelia Research Campus, Ashburn VA. These sequences can be found under the SRA BioProject PRJNA762862.

Sample ID	Collection Date	Collection Location	Generation	Organ	Library Prep Method	Sequencing Method	# Reads	Accession #
Tulm_Fund_SG_2	4/22/19	JRC	1	SG	WGB	Illumina PE150	8475508, 5308849	SRR15871517
Tulm_Fund_SG_4	4/22/19	JRC	1	SG	WGB	Illumina PE150	6087930, 6250323	SRR15871516

Tulm_Fund_SG_5	4/22/19	JRC	1	SG	WGB	Illumina PE150	7474183, 7147731	SRR15871515
Tulm_Fund_Carc_2	4/22/19	JRC	1	Carcass	WGB	Illumina PE150	6208251, 6194859	SRR15871514
Tulm_Fund_Carc_4	4/22/19	JRC	1	Carcass	WGB	Illumina PE150	7453030, 6095776	SRR15871513
Tulm_Fund_Carc_5	4/22/19	JRC	1	Carcass	WGB	Illumina PE150	8399343, 7332616	SRR15871512
Tulm_2ndGen_SG_2_1	4/22/19	JRC	2	SG	WGB	Illumina PE150	6902051, 7037142	SRR15871511
Tulm_2ndGen_SG_2_2	4/22/19	JRC	2	SG	WGB	Illumina PE150	6888742, 6997123	SRR15871510
Tulm_2ndGen_SG_2_3	4/22/19	JRC	2	SG	WGB	Illumina PE150	6049169, 6696157	SRR15871509

Table S4 - Details of biological samples, sequence files, and SRA accession numbers for *Acyrthosiphon pisum* RNA-sequencing. The aphid strain used was LSR1 (Caillaud et al., 2002), originally collected in the vicinity of Ithaca, NY, USA in summer 1998. Aphids were grown on broad bean plants in the laboratory at Janelia Reseach Campus and dissected for these samples on 21 February 2021. Sequences can be found under SRA BioProject PRJNA762703.

Sample ID	Collection Date	Collection Location	Generation	Organ	Library Prep Method	Sequencing Method	# Reads	Accession #
SG1	1998	Ithaca, NY, USA	1	SG	WGB	Illumina PE150	1273082, 5724222	SRR15862168
SG2	1998	Ithaca, NY, USA	1	SG	WGB	Illumina PE150	1557673, 6606339	SRR15862167
SG3	1998	Ithaca, NY, USA	1	SG	WGB	Illumina PE150	1199959, 5221105	SRR15862166
SG4	1998	Ithaca, NY, USA	1	SG	WGB	Illumina PE150	1159521, 5169430	SRR15862165
carc1	1998	Ithaca, NY, USA	1	Carcass	WGB	Illumina PE150	998879, 4363153	SRR15862164
carc2	1998	Ithaca, NY, USA	1	Carcass	WGB	Illumina PE150	1185062, 5433749	SRR15862163
carc3	1998	Ithaca, NY, USA	1	Carcass	WGB	Illumina PE150	1045749, 4901408	SRR15862162

Table S5 – SRA accession numbers for Genomes downloaded from NCBI.

Species	Original genomes Genbank assembly accession or alternative location	Publication source of each genome	Manually corrected BRAKER Annotation	TRINITY assembly
Acyrthosiphon pisum	https://bipaa.genouest.org/sp/acyrthosiphon_pisum/download/genome/JIC1_1.0/	(Mathers et al., 2021)	Apis.Augustus.updated_w_annots.22xii21.gff3	apis.Trinity.fasta.gz
Aphis gossypi	GCF_004010815.1	(Quan et al., 2019)	Agos.Augustus.updated_w_annots.24vii21.gff3	agos.Trinity.fasta.gz
Bemisia tabaci	GCA_001854935.1	(Chen et al., 2016)	Btab.Augustus.updated_w_annots.7vii21.gff3	

Cinara cedri	GCA_902439185.1	(Julca et al., 2020)	Cced.Augustus.updated_w_annots.7vii21.gff3	cced.Trinity.fasta.gz
Daktulosphaira vitifoliae	https://bipaa.genouest.org/sp/daktulosphaira_vitifoliae/download/genome/v3.1/Dv_mitochondrial_genome.fa	(Rispe et al., 2020)	Dvit.Augustus.updated_w_annots.7vii21.gff3	
Diaphorina citri	GCA_000475195.1	(Saha et al., 2017)	Dcit.Augustus.updated_w_annots.7vii21.gff3	
Diuraphis noxia	GCA_001186385.1	(Nicholson et al., 2015) (Zhang et al., 2014)	Dnox.Augustus.updated_w_annots.7vii21.gff3	dnox.Trinity.fasta.gz
Ericerus pela	GCA_011428145.1	(Yang et al., 2019)	Epel.Augustus.updated_w_annots.7vii21.gff3	
Eriosoma lanigerum	GCA_013282895.1	(Biello et al., 2021)	Elan.Augustus.updated_w_annots.7vii21.gff3	elan.Trinity.fasta.gz
Hormaphis cornu	GCA_017140985.1	(Korgaonkar et al., 2021)	Augustus.updated_w_annots.19viii21_final.gff3	hcor.Trinity.fasta.gz
Laodelphax striatella	GCA_003335185.2	(Zhu et al., 2017)	Lstr.Augustus.updated_w_annots.7vii21.gff3	
Maconellicoccus hirsutus	GCA_003261595.1	(Kohli et al., 2021)	Mhir.Augustus.updated_w_annots.7vii21.gff3	
Melanaphis sacchari	GCA_002803265.2	https://data.nal.usda.gov/dataset/melanaphis-sacchari-strainlsu-and-endosymbiont-genome-sequencing-and-assembly	Msac.Augustus.updated_w_annots.7vii21.gff3	msac.Trinity.fasta.gz
Myzus persicae	https://bipaa.genouest.org/sp/myzus_persicae/download/genome/v2.0/	(Mathers et al., 2021)	Mper.Augustus.updated_w_annots.13xii21.gff3	mper.Trinity.fasta.gz
Nilaparvata lugens	GCA_000757685.1	(Xue et al., 2014)	Nlug.Augustus.updated_w_annots.7vii21.gff3	
Pachypsylla venusta	GCA_012654025.1	(Y. Li et al., 2020)	Pven.Augustus.updated_w_annots.7vii21.gff3	
Pentalonia nigronervosa	GCA_014851325.1	(Mathers et al., 2020)	Pnig.Augustus.updated_w_annots.7vii21.gff3	pnig.Trinity.fasta.gz
Phenacoccus solenopsis	GCA_009761765.1	(M. Li et al., 2020)	Psol.Augustus.updated_w_annots.7vii21.gff3	
Rhopalosiphum maidis	GCF_003676215.2	(Chen et al., 2019)	Rmai.Augustus.updated_w_annots.7vii21.gff3	rmai.Trinity.fasta.gz
Sipha flava	GCA_003268045.1	https://data.nal.usda.gov/dataset/crop-rotational-diversity-affects-soil-microbiomes	Sfla.Augustus.updated_w_annots.7vii21.gff3	sfla.Trinity.fasta.gz
Tetraneura ulmi	JAIUCT000000000	NA	Tulm.Augustus.updated_w_annots.7vii21.gff3	tulm.Trinity.fasta.gz
Trialeurodes vaporariorum	GCA_011764245.1	(Xie et al., 2020)	Tvap.Augustus.updated_w_annots.7vii21.gff3	

Table S6 – SRA accession numbers for RNAseq samples downloaded from NCBI. See separate file “S6_RNAseq_SRA_accessions.xlsx”.

Figure 1

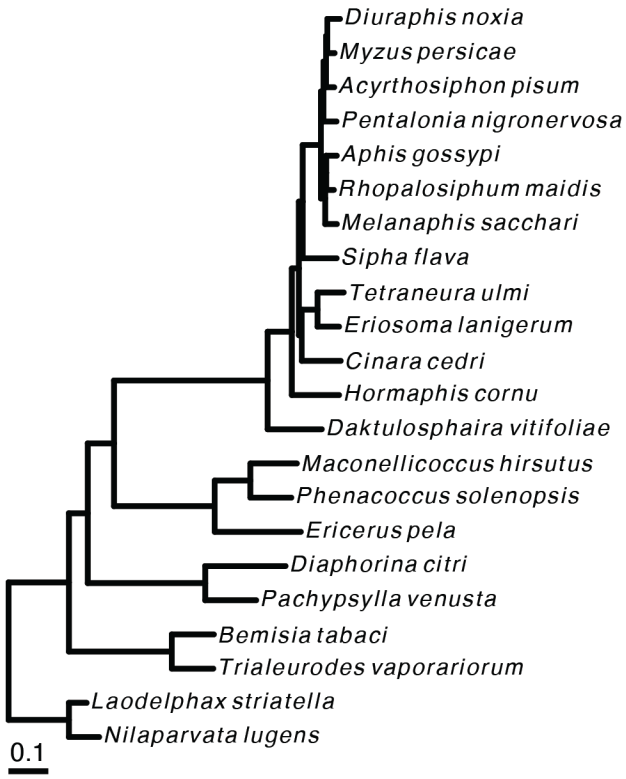

	BLAST	HMMER	Classifier	HMMER–within
Aphidoidae	0	0	15	12
	2	1	117	59
	1	3	121	69
	1	0	64	31
	3	2	29	15
	2	3	65	32
	1	0	27	40
	0	1	3	8
	1	53	279	69
	0	3	27	23
	4	15	70	41
	510	458	653	446
Phylloxeroidae	0	0	69	62
Coccoidea	0	0	74	91
	0	0	26	24
	0	0	2	14
Psylloidea	0	0	0	0
	0	0	0	0
Aleyrodoidea	0	0	0	0
	0	0	0	0
Fulgoroidea	0	0	0	0
	0	0	0	0

Figure 2

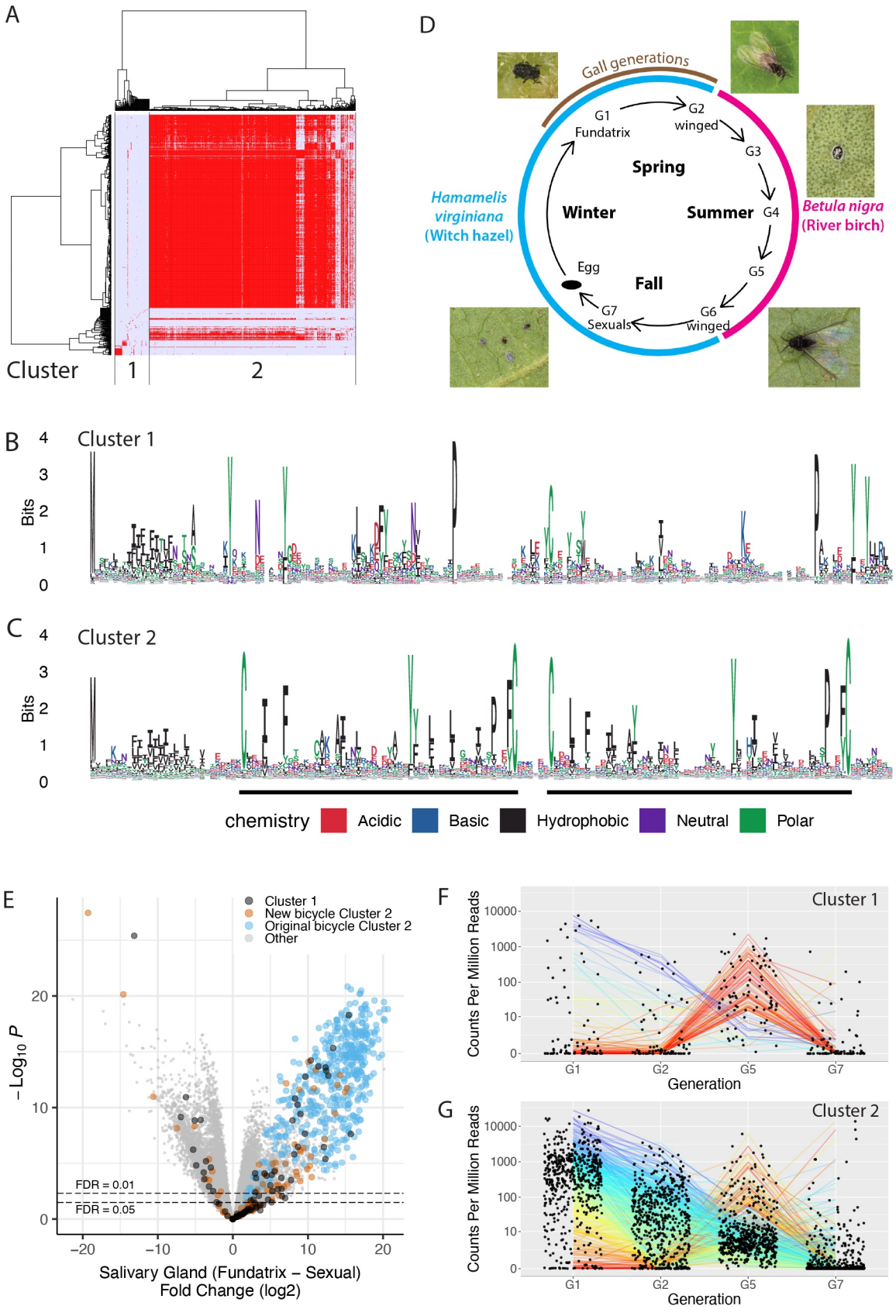
A
Cluster
1
2
D
Gall generations
G1
Fundatrix
G2
winged
G3
Spring
Summer
G4
G5
G6
winged
G7
Sexuals
Egg
Fall
Winter
Hamamelis virginiana
(Witch hazel)
Betula nigra
(River birch)
B
Cluster 1
Bits
C
Cluster 2
Bits
chemistry
Acidic
Basic
Hydrophobic
Neutral
Polar
E
Cluster 1
New bicycle Cluster 2
Original bicycle Cluster 2
Other
$-\text{Log}_{10}\ P$
FDR = 0.01
FDR = 0.05
Salivary Gland (Fundatrix – Sexual)
Fold Change (log2)
F
Cluster 1
Counts Per Million Reads
Generation
G
Cluster 2
Counts Per Million Reads
Generation

Figure 3

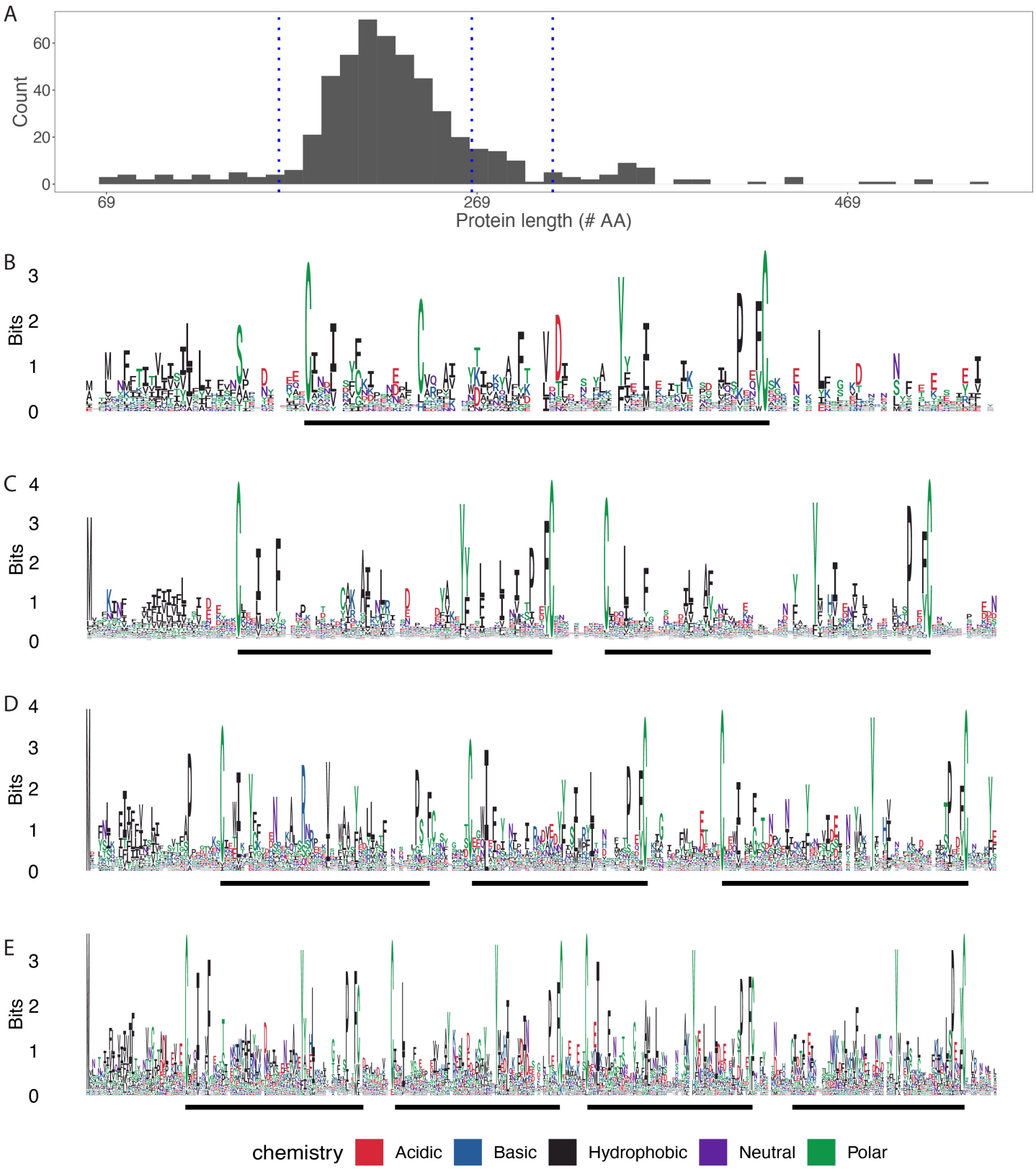
A
Count
60
40
20
0
69
269
469
Protein length (# AA)
B
Bits
3
2
1
0
C
Bits
4
3
2
1
0
D
Bits
4
3
2
1
0
E
Bits
3
2
1
0
chemistry
Acidic
Basic
Hydrophobic
Neutral
Polar

Figure 4

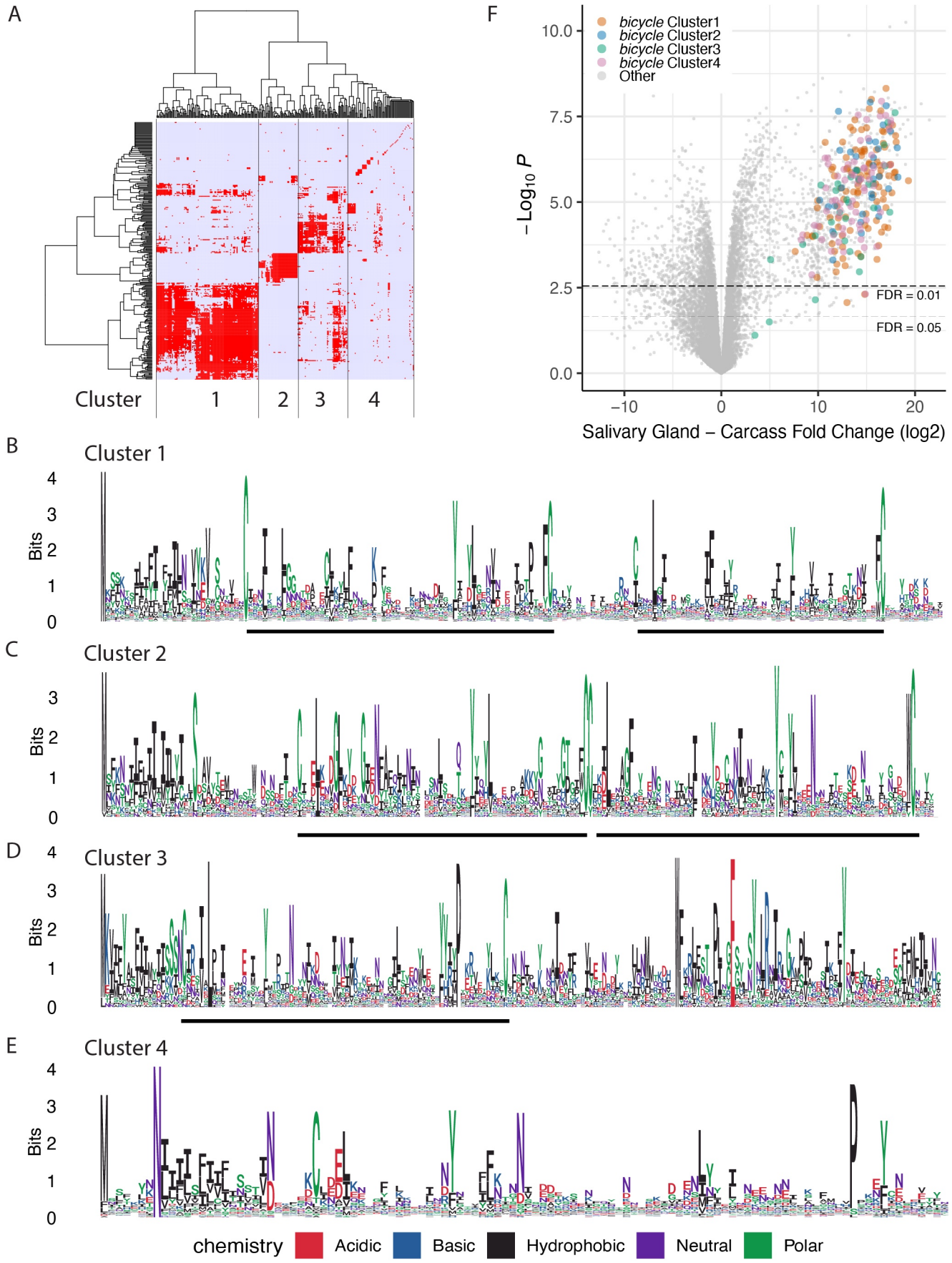
A
Cluster
1
2
3
4
F
bicycle Cluster1
bicycle Cluster2
bicycle Cluster3
bicycle Cluster4
Other
FDR = 0.01
FDR = 0.05
−Log10 P
Salivary Gland – Carcass Fold Change (log2)
B
Cluster 1
C
Cluster 2
D
Cluster 3
E
Cluster 4
Bits
chemistry
Acidic
Basic
Hydrophobic
Neutral
Polar

Figure 5

A

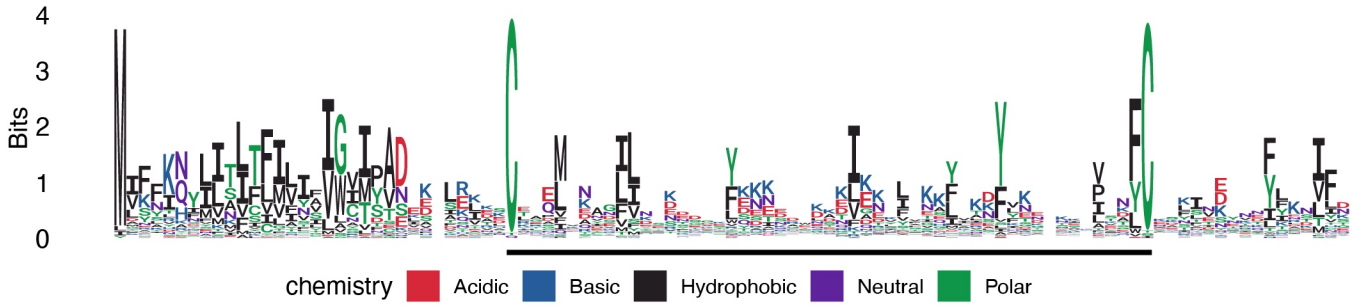
Bits
4
3
2
1
0
chemistry
Acidic
Basic
Hydrophobic
Neutral
Polar

B

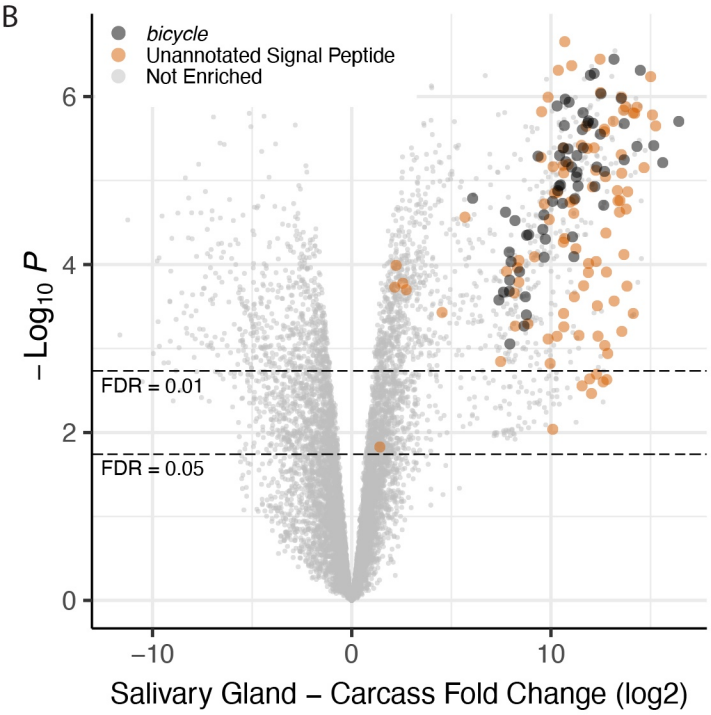
bicycle
Unannotated Signal Peptide
Not Enriched
FDR = 0.01
FDR = 0.05
−Log10 P
6
4
2
0
−10
0
10
Salivary Gland − Carcass Fold Change (log2)

Figure 6

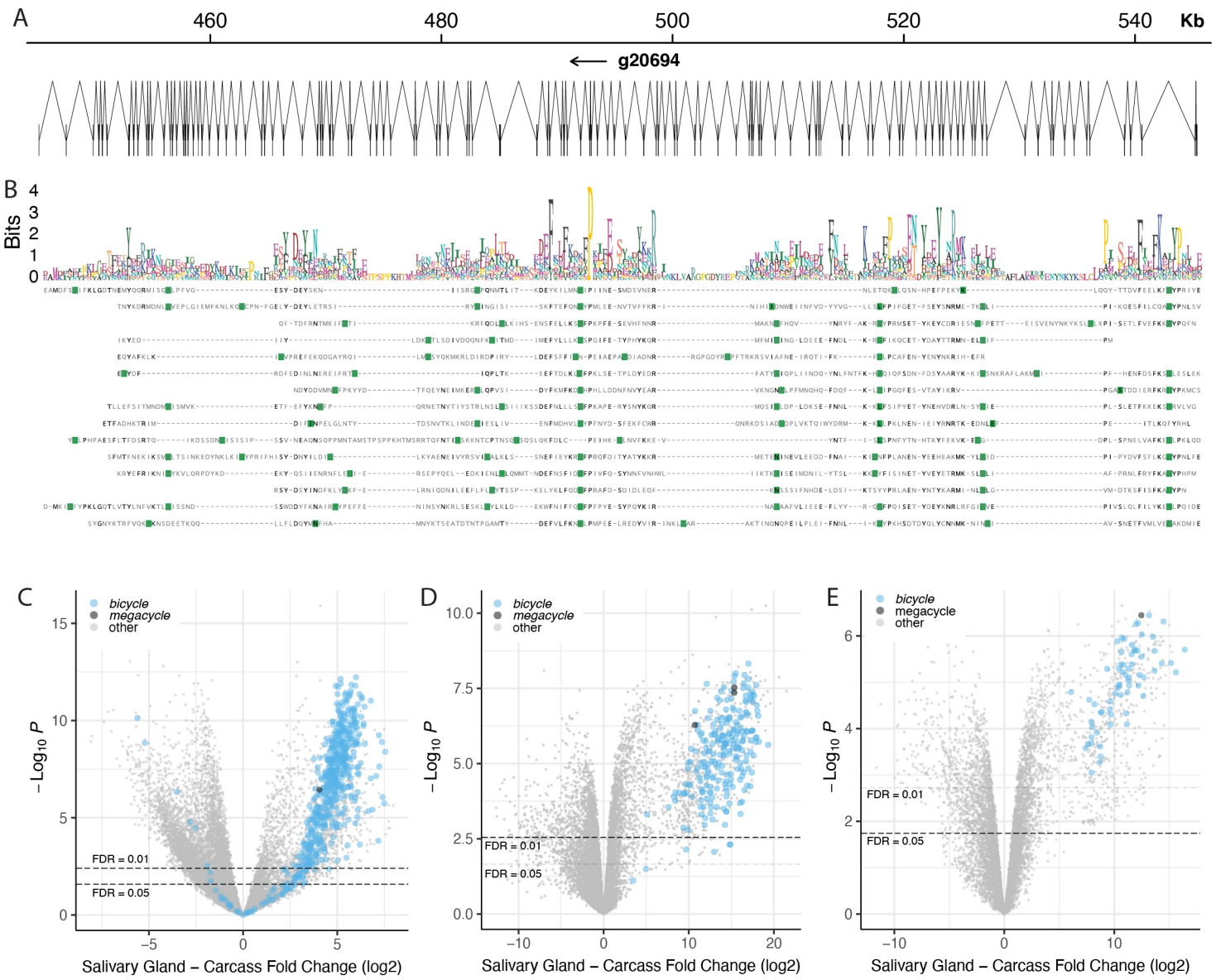
A
460
480
500
520
540
Kb
g20694
B
Bits
C
bicycle
megacycle
other
FDR = 0.01
FDR = 0.05
−Log10 P
Salivary Gland − Carcass Fold Change (log2)
D
bicycle
megacycle
other
FDR = 0.01
FDR = 0.05
−Log10 P
Salivary Gland − Carcass Fold Change (log2)
E
bicycle
megacycle
other
FDR = 0.01
FDR = 0.05
−Log10 P
Salivary Gland − Carcass Fold Change (log2)

Figure S1

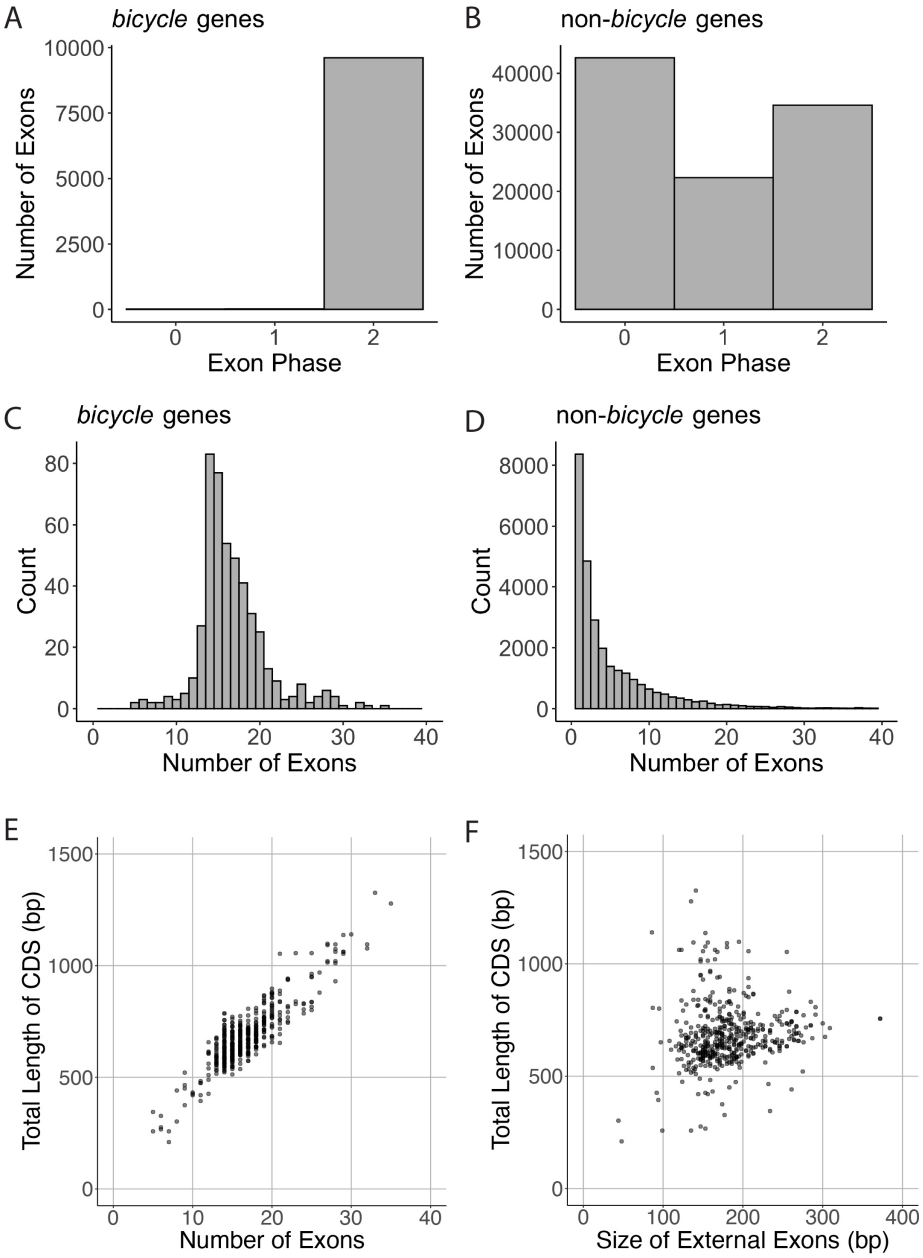
A
bicycle genes
Number of Exons
10000
7500
5000
2500
0
0
1
2
Exon Phase
B
non-bicycle genes
Number of Exons
40000
30000
20000
10000
0
0
1
2
Exon Phase
C
bicycle genes
Count
80
60
40
20
0
0
10
20
30
40
Number of Exons
D
non-bicycle genes
Count
8000
6000
4000
2000
0
0
10
20
30
40
Number of Exons
E
Total Length of CDS (bp)
1500
1000
500
0
0
10
20
30
40
Number of Exons
F
Total Length of CDS (bp)
1500
1000
500
0
0
100
200
300
400
Size of External Exons (bp)

Figure S2

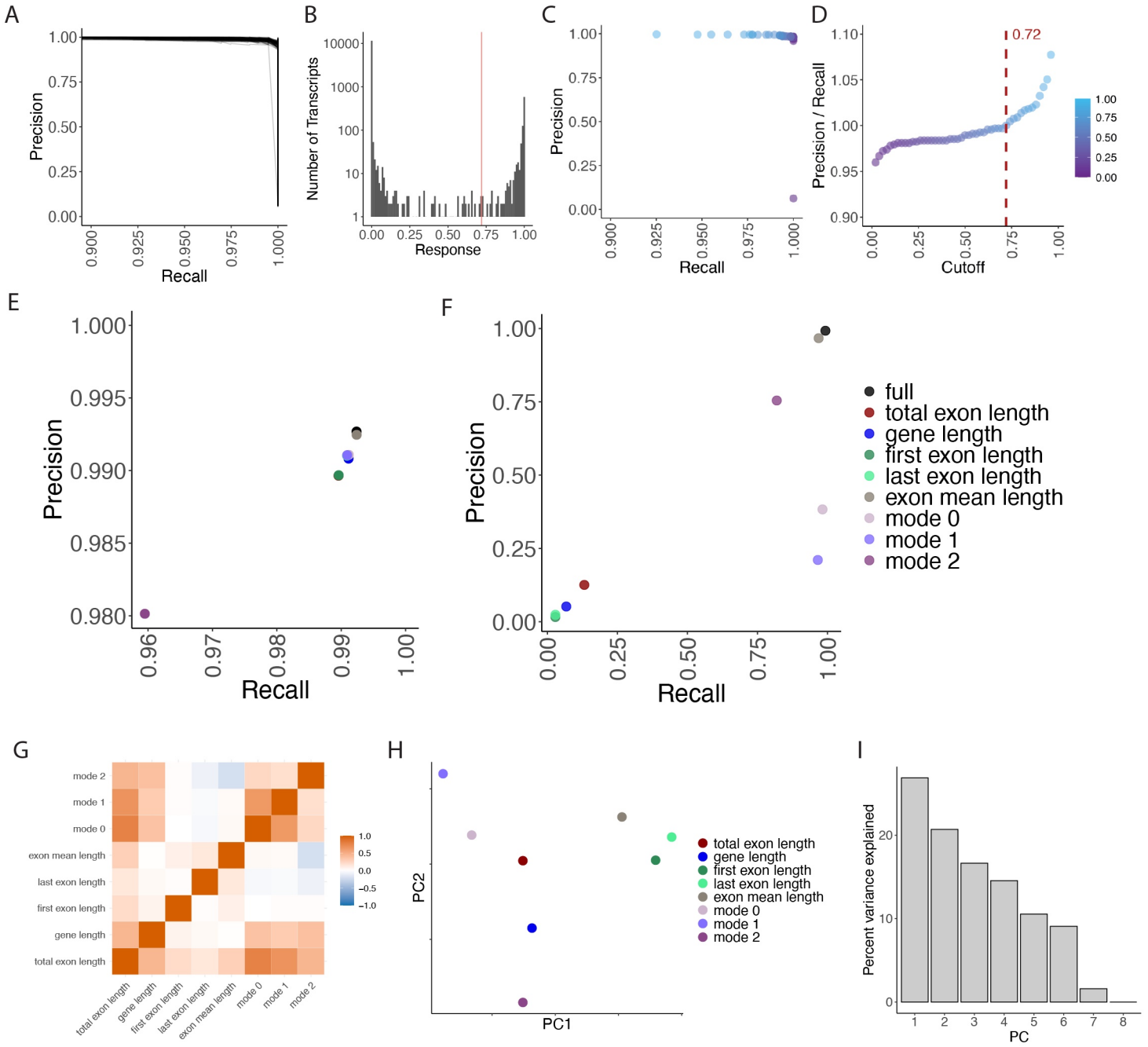
A
Precision
Recall
B
Number of Transcripts
Response
C
Precision
Recall
D
Precision / Recall
Cutoff
0.72
E
Precision
Recall
F
Precision
Recall
full
total exon length
gene length
first exon length
last exon length
exon mean length
mode 0
mode 1
mode 2
G
mode 2
mode 1
mode 0
exon mean length
last exon length
first exon length
gene length
total exon length
H
PC1
PC2
total exon length
gene length
first exon length
last exon length
exon mean length
mode 0
mode 1
mode 2
I
Percent variance explained
PC

Figure S3

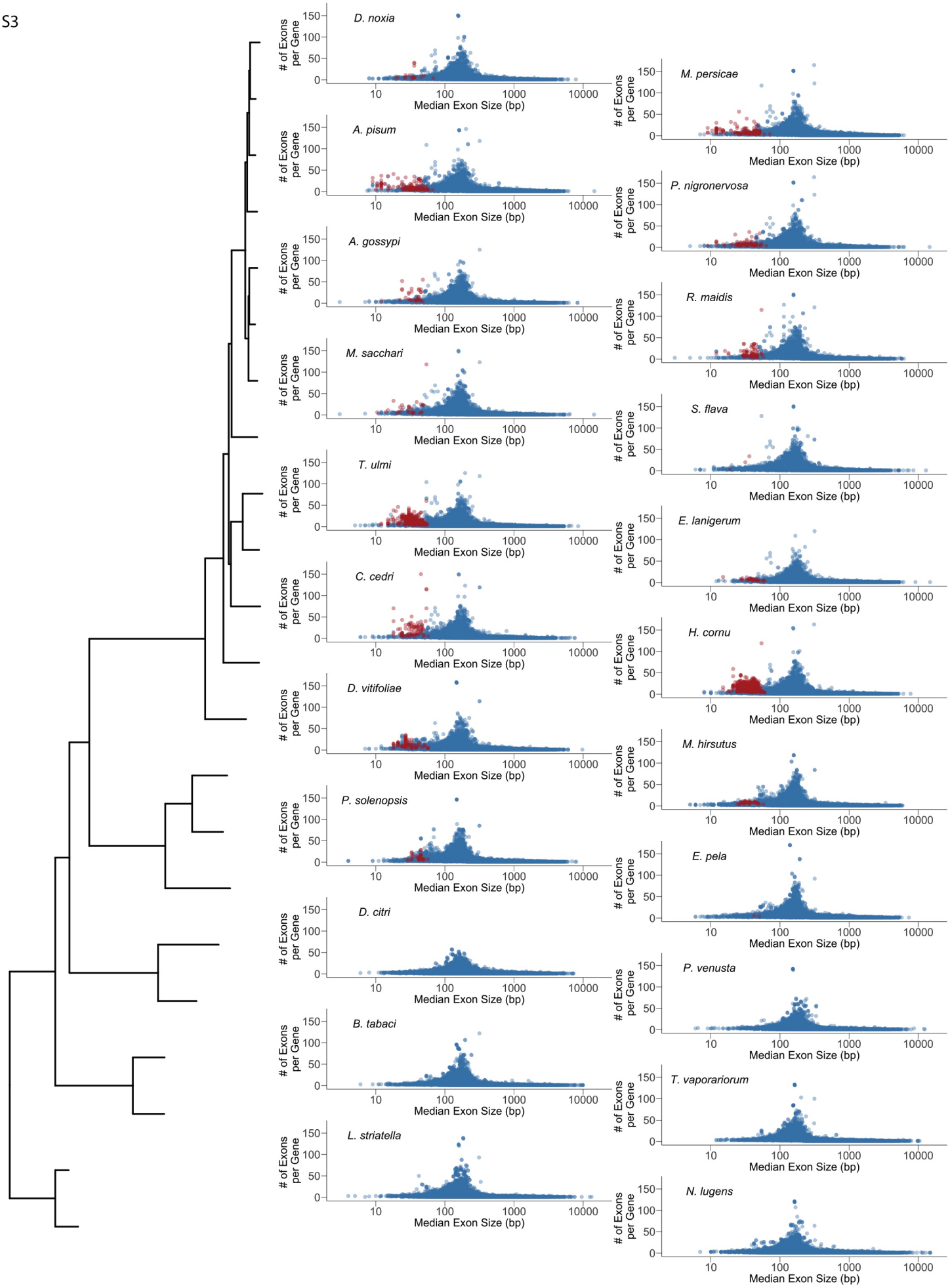
D. noxia
A. pisum
A. gossypi
M. sacchari
T. ulmi
C. cedri
D. vitifoliae
P. solenopsis
D. citri
B. tabaci
L. striatella
M. persicae
P. nigronervosa
R. maidis
S. flava
E. lanigerum
H. cornu
M. hirsutus
E. pela
P. venusta
T. vaporariorum
N. lugens
# of Exons per Gene
Median Exon Size (bp)
0
50
100
150
10
100
1000
10000

Figure S4

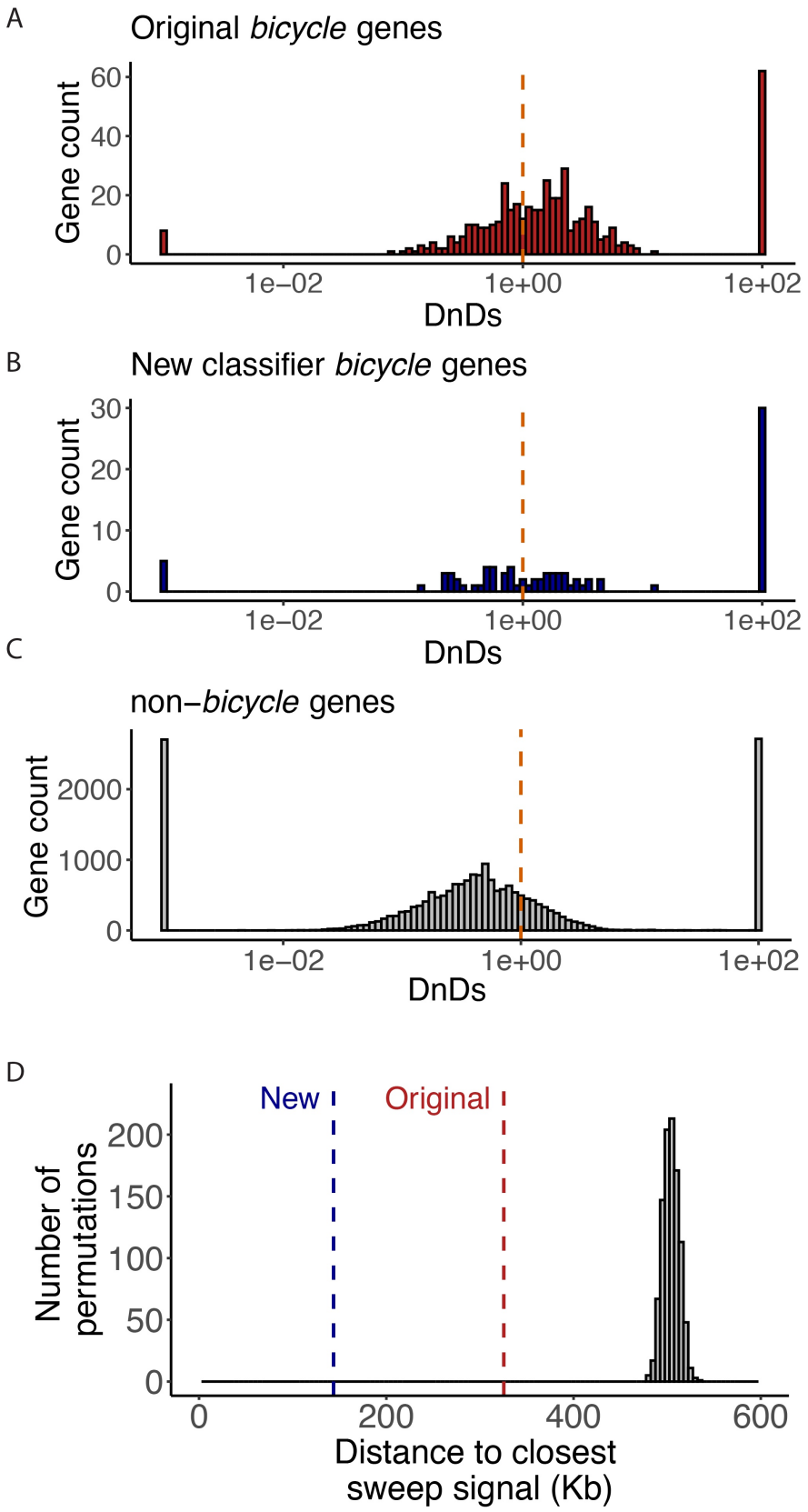
A
Original *bicycle* genes
Gene count
60
40
20
0
1e−02
1e+00
1e+02
DnDs
B
New classifier *bicycle* genes
Gene count
30
20
10
0
1e−02
1e+00
1e+02
DnDs
C
non−*bicycle* genes
Gene count
2000
1000
0
1e−02
1e+00
1e+02
DnDs
D
New
Original
Number of permutations
200
150
100
50
0
0
200
400
600
Distance to closest sweep signal (Kb)

Figure S5

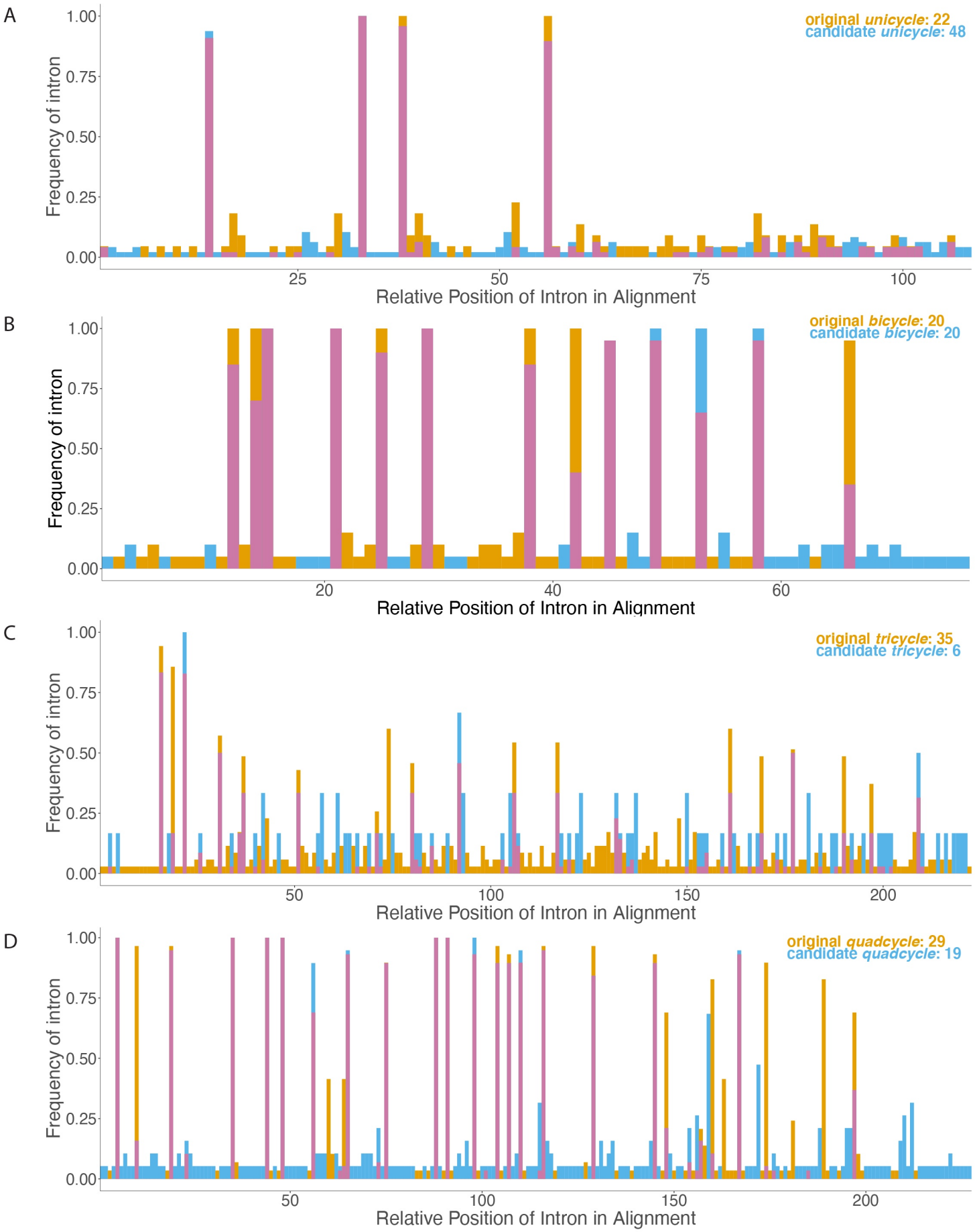
A
original unicycle: 22
candidate unicycle: 48
Frequency of intron
1.00
0.75
0.50
0.25
0.00
25
50
75
100
Relative Position of Intron in Alignment
B
original bicycle: 20
candidate bicycle: 20
Frequency of intron
1.00
0.75
0.50
0.25
0.00
20
40
60
Relative Position of Intron in Alignment
C
original tricycle: 35
candidate tricycle: 6
Frequency of intron
1.00
0.75
0.50
0.25
0.00
50
100
150
200
Relative Position of Intron in Alignment
D
original quadcycle: 29
candidate quadcycle: 19
Frequency of intron
1.00
0.75
0.50
0.25
0.00
50
100
150
200
Relative Position of Intron in Alignment

Figure S6

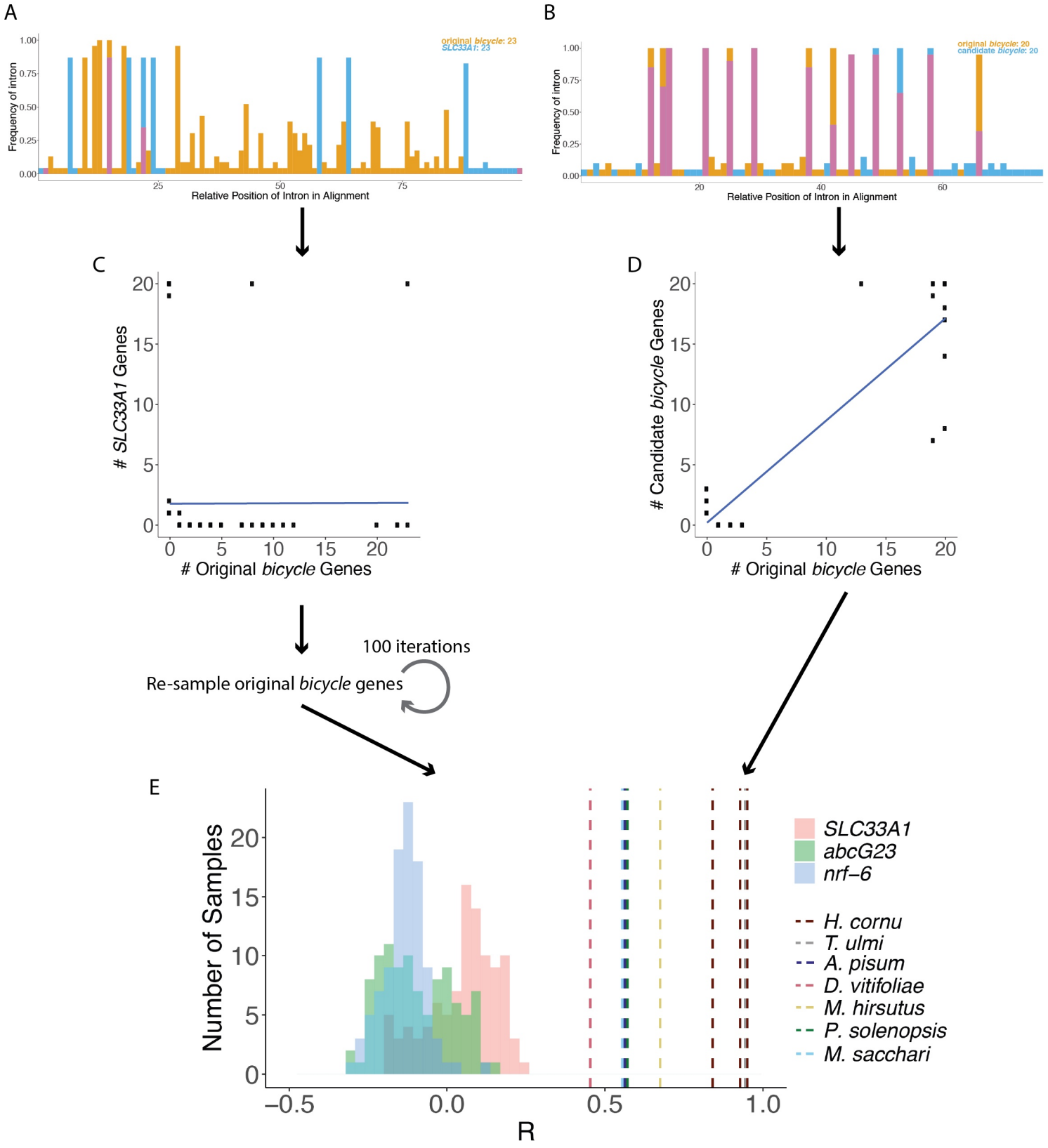
A
original bicycle: 23
SLC33A1: 23
Frequency of intron
Relative Position of Intron in Alignment
B
original bicycle: 20
candidate bicycle: 20
Frequency of intron
Relative Position of Intron in Alignment
C
SLC33A1 Genes
Original bicycle Genes
D
Candidate bicycle Genes
Original bicycle Genes
100 iterations
Re-sample original bicycle genes
E
Number of Samples
R
SLC33A1
abcG23
nrf–6
H. cornu
T. ulmi
A. pisum
D. vitifoliae
M. hirsutus
P. solenopsis
M. sacchari

Figure S7

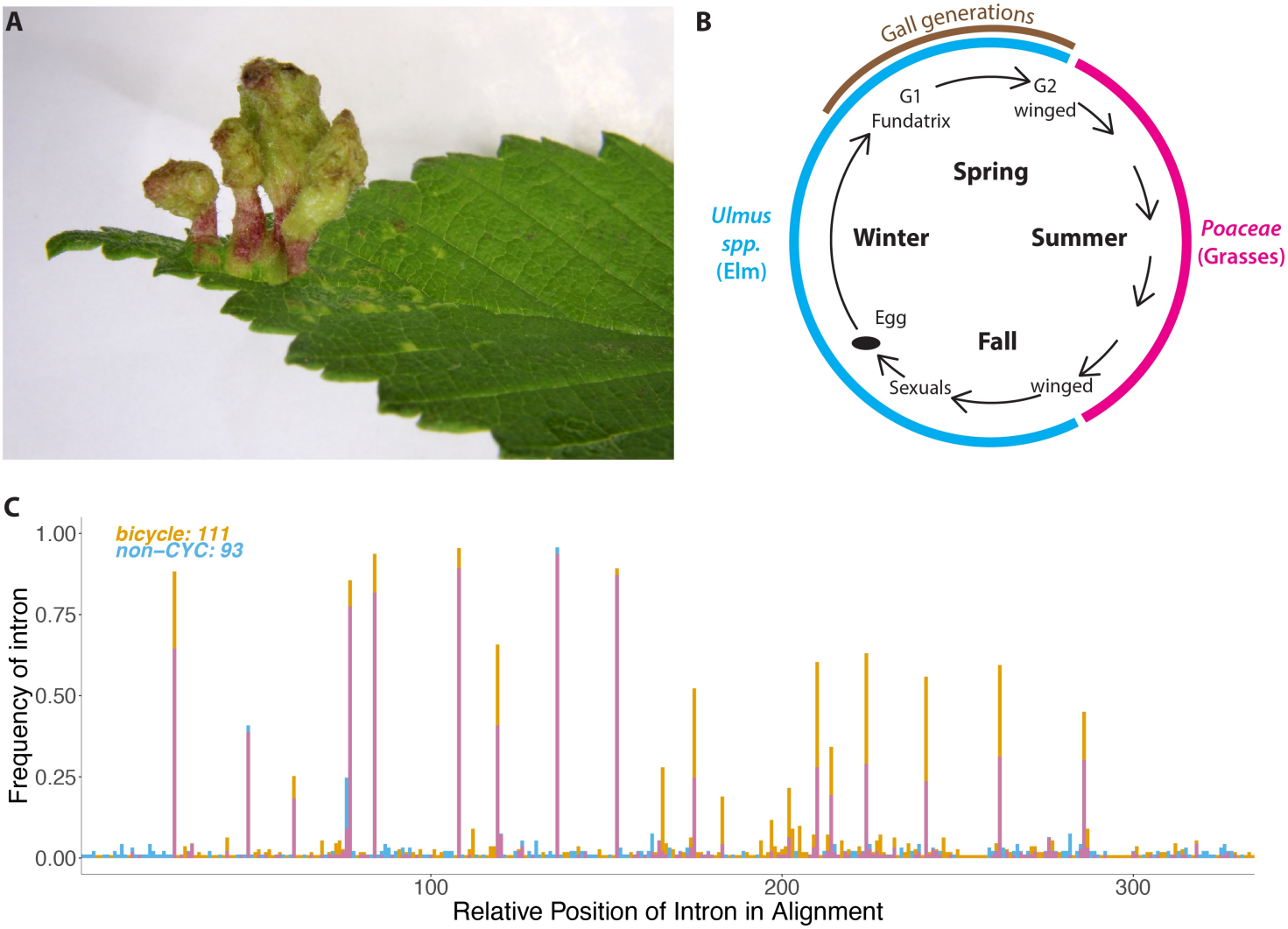
A
B
Gall generations
G1
Fundatrix
G2
winged
Spring
Summer
Winter
Fall
Egg
Sexuals
winged
Ulmus
spp.
(Elm)
Poaceae
(Grasses)
C
bicycle: 111
non−CYC: 93
Frequency of intron
1.00
0.75
0.50
0.25
0.00
100
200
300
Relative Position of Intron in Alignment

Figure S8

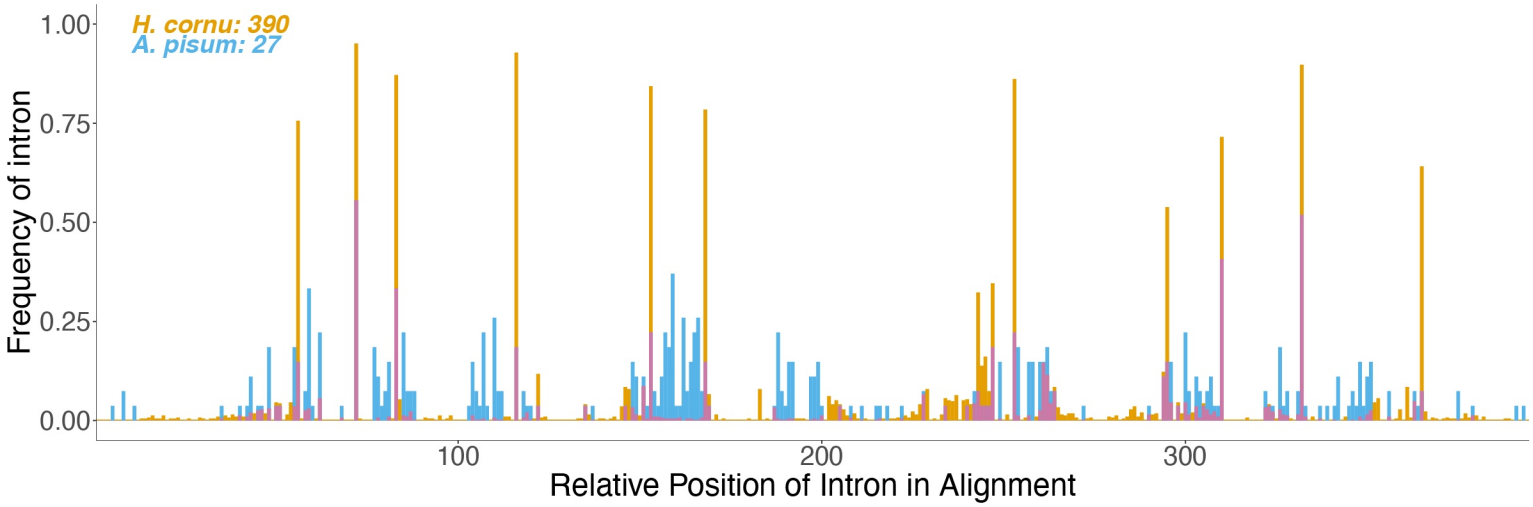
H. cornu: 390
A. pisum: 27
1.00
0.75
0.50
0.25
0.00
Frequency of intron
100
200
300
Relative Position of Intron in Alignment

Figure S9

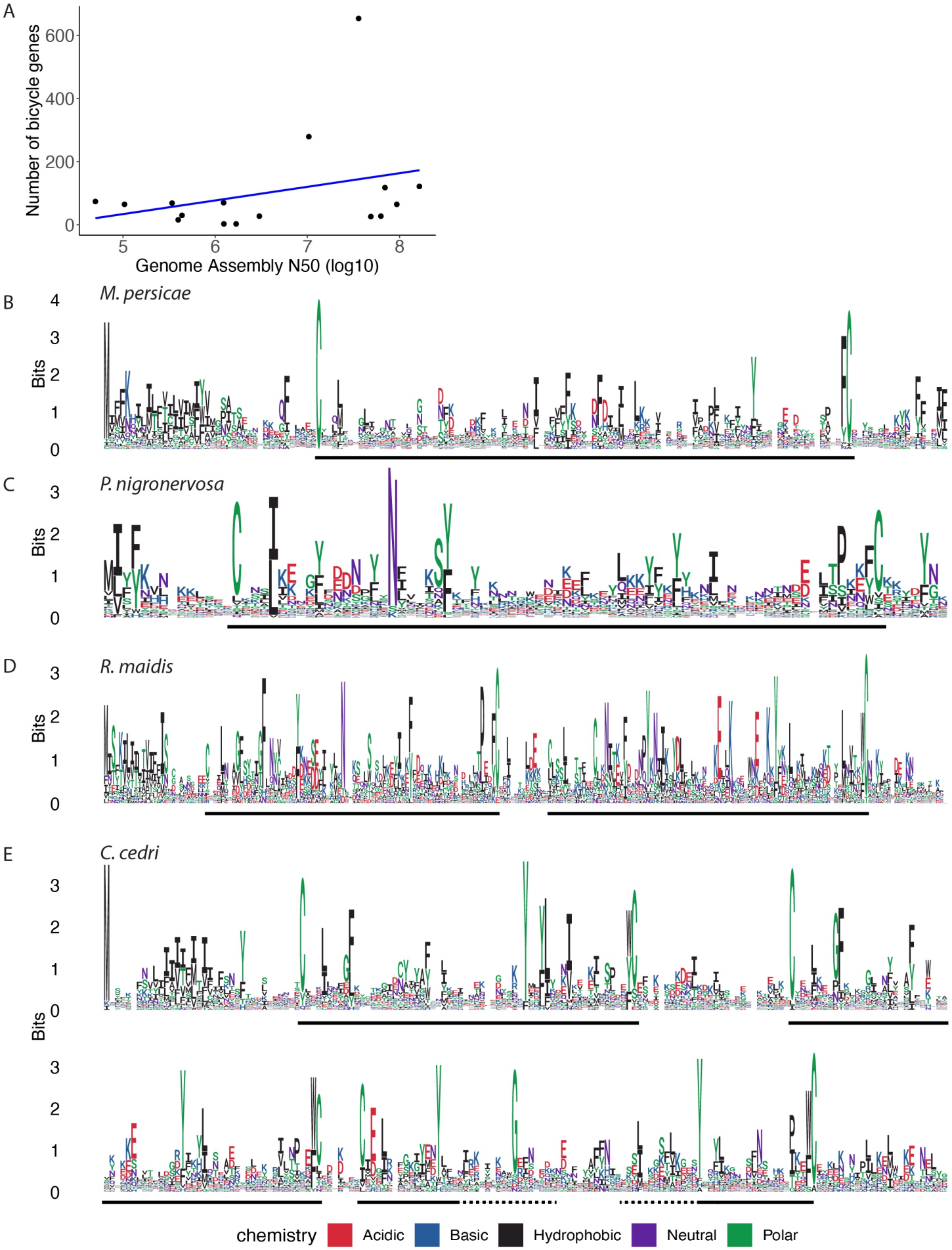
A
Number of bicycle genes
0
200
400
600
5
6
7
8
Genome Assembly N50 (log10)
B
M. persicae
C
P. nigronervosa
D
R. maidis
E
C. cedri
Bits
chemistry
Acidic
Basic
Hydrophobic
Neutral
Polar

Figure S10

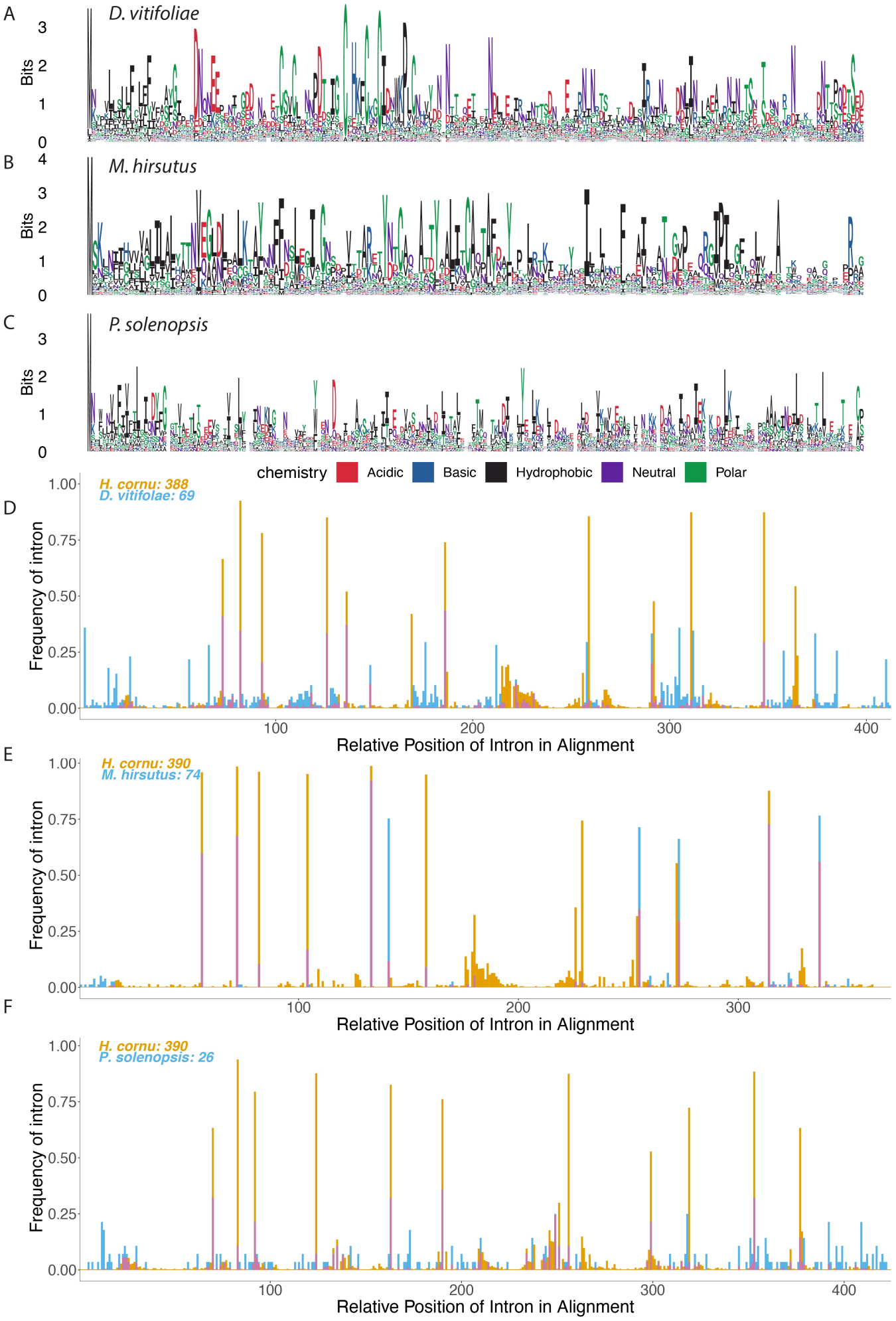
A
D. vitifoliae
B
M. hirsutus
C
P. solenopsis
Bits
chemistry
Acidic
Basic
Hydrophobic
Neutral
Polar
D
H. cornu: 388
D. vitifolae: 69
E
H. cornu: 390
M. hirsutus: 74
F
H. cornu: 390
P. solenopsis: 26
Frequency of intron
Relative Position of Intron in Alignment

Figure S11

A

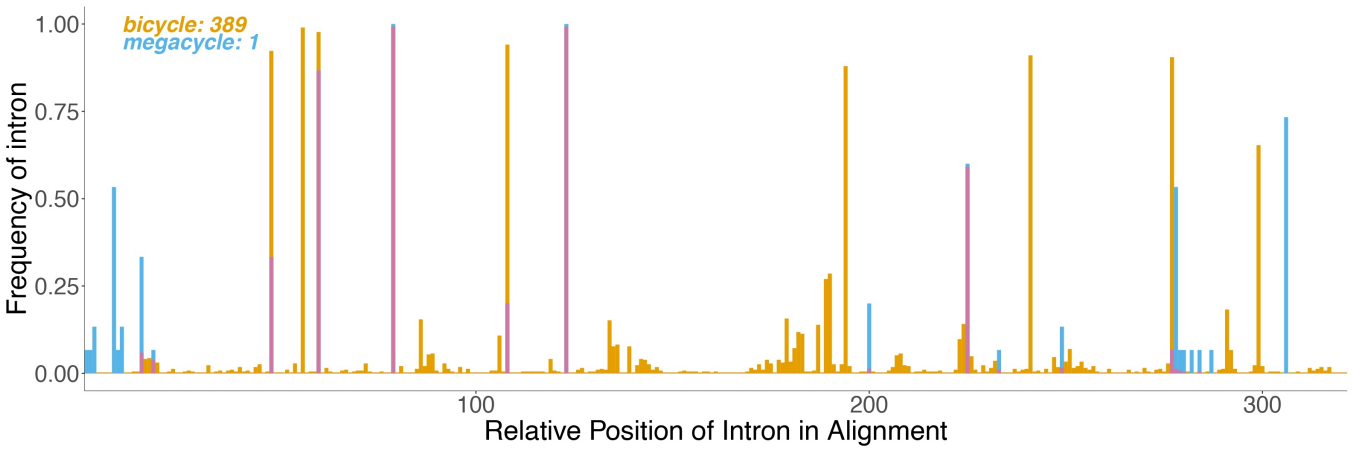
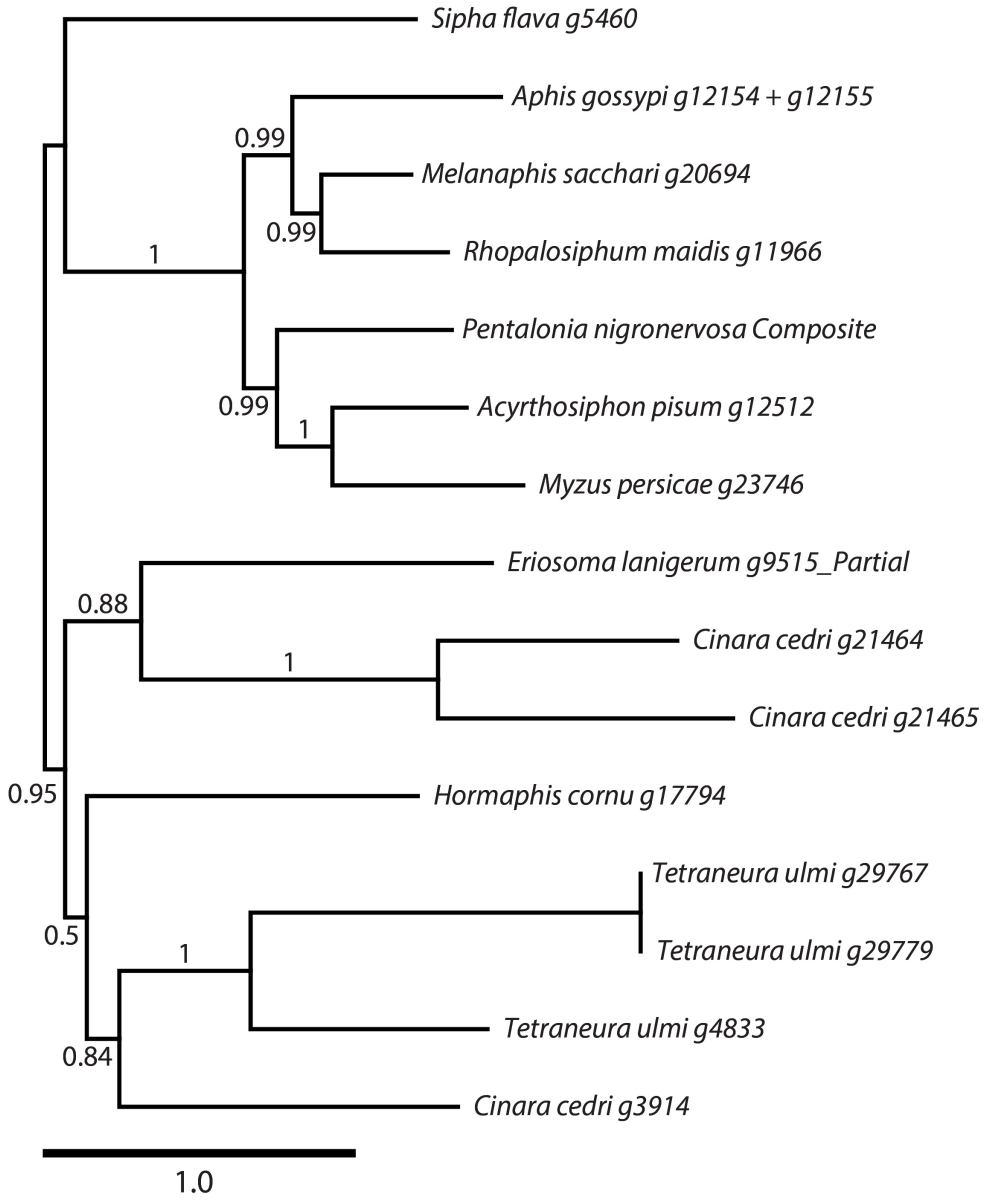
B